The "Escarot" gas seep, French Massif Central: CO2 discharge from a quiescent volcanic system – Characterization and quantification of gas emissions

Frédérick Gal, Steve Leconte, Alain Gadalia

The "Escarot" gas seep, French Massif Central: CO_2 discharge from a quiescent volcanic system – Characterization and quantification of gas emissions.

Authors:

Gal F.[1*], Leconte S.[2], Gadalia A.[1]

1: BRGM, F-45060 Orléans, France

2: BRGM, F-63170 Aubière, France

*: corresponding author: f.gal@brgm.fr

Abstract

Natural CO_2 emissions from the volcanic rocks of the French Massif Central are poorly constrained. It is of interest better to assess the emission of such non-anthropogenic gases that may significantly contribute to the global carbon budget. We quantified the CO_2 emissions to the atmosphere in a small area (0.052 km²) located in the Massif Central close to Lake Pavin, the most recent volcanic edifice in metropolitan France. The specific character of this area, known as the Escarot mofette, was earlier studied for soil-gas concentrations only. In June 2017, we used the accumulation chamber method for measuring CO_2 flux and related O_2 depletion in the gases emitted at the soil/atmosphere interface, resulting in 176 data acquisitions over four days. In addition, 44 soil-gas concentration measurements were made at selected locations. CO_2 emission rates are estimated at 8,100±1,800 tons/year of deep-seated CO_2 and at 660±440 tons/year of biologically produced CO_2. The uncertainty on these evaluations comes from the high-frequency variability of CO_2 efflux in the more emissive areas and from the occurrence of heavy precipitation events. Though unexpected, these events were used for quantifying the decreases in CO_2 efflux, which were as high as 500% over a few hours or even days in some locations. However, repeat acquisitions performed under more favourable weather conditions showed errors of commonly accepted amplitude (±15%). The area showed several degassing centres aligned along a NNW-SSE direction that correlates well with known geological structures, proving the ability of soil-gas methods to map hidden faults. The whole area is characterized by strong CO_2 enrichment and related O_2 depletion, but it is nonetheless possible to detect areas influenced by the rise of deep-seated gases and a few peripheral areas where biological processes dominate (CO_2 up to 10% vol.). This study of gas emissions in a non-urban area also provides complementary information that is of use when extrapolated to similar structures in urban

areas, where the occurrence of such gas releases, and its potential hazard may be more difficult to assess.

Highlights

- Spatial and geochemical characterizations of a CO_2 gas seep in the French Massif Central.
- Magmatic CO_2 gas emissions into the atmosphere evaluated at around 8,100 tons/year.
- CO_2 gas flux is successfully used for mapping hidden faults.
- Decrease in gas flux of up to 500% after the occurrence of heavy precipitation events.
- Use of the O_2-decrease parameter in gas efflux better to assess the strength of gas emissions to the surface.

Keywords

Carbon dioxide – gas flux – released amounts – meteorological parameters – degassing structures

1. Introduction

The Earth's natural degassing induces the release into the atmosphere of many gas species, including some "greenhouse gases" (*e.g.* N_2O, CH_4, CO_2 or H_2O). Volcanic structures obviously play an important role in this degassing process, either during explosive (eruptive) phases, or during quiescent (non-eruptive) periods (*e.g.* Halmer *et al.*, 2002). Such degassing may be diffuse, or focused through volcanic edifices, hydrothermal manifestations, or gas vents, the last two commonly being related to faults (*e.g.* Judd, 2005; Burton *et al.*, 2013; Etiope, 2015). The budgets of carbon emissions into the atmosphere have been assessed since the 1980s (*e.g.* Werner *et al.*, 2000; Kerrick, 2001; Mörner and Etiope, 2002 and references therein) and are regularly refined (*e.g.* Holloway *et al.*, 2007; Lewicki *et al.*, 2007), or the ongoing investigations on French active volcanoes by Boudoire *et al.*, 2017 and Liuzzo *et al.*, 2015). Such carbon-emission budgets should include the release of CO_2 as a gas phase as well as the amounts of CO_2 dissolved in aquifers or lakes that may represent a non-negligible contribution (*e.g.* Sorey *et al.*, 1998).

Even during periods of quiescence, the release of gases, especially CO_2, can be high (*e.g.* Werner *et al.*, 2009). Volcanic structures are not only characterized by the presence of degassing structures, such as fumaroles or gas vents, and diffuse degassing processes, but commonly also by the existence of thermal anomalies in the soil and of hot springs or steam emissions (*e.g.* Frondini *et al.*, 2004). This is often the case when the quiescence period has been relatively short at a geological scale, such as around 130 years at Pantelleria Island, Sicily (Favara *et al.*, 2001), around 400 years at Furnas volcano, Azores (Pedone *et al.*, 2015) and around 600 years at Mammoth Mountains, California (Sorey *et al.*, 1998). Nevertheless, some volcanic edifices that have been quiescent for a similar duration will have no thermal

anomalies or fumarolic activity (Hakkoda, Japan; Hernández-Perez *et al.*, 2003) and even no gas emissions into the atmosphere (Mount Fuji, Japan; Notsu *et al.* (2006). The longer the duration of the quiescent period, the fewer thermal anomalies there will be, such as in the West European rift and its associated volcanic structures in France and Germany.

Here, however, the absence of high-temperature manifestations does not mean that there are no gas releases, but these are less commonly quantified. When they are, quantification may refer to the gas flux in water bodies, such as a flux of 1450±350 $g.m^{-2}.y^{-1}$ of magmatic CO_2 in the German Laacher See (Aeschbach-Hertig *et al.*, 1996), or a flux of 170±60 $g.m^{-2}.y^{-1}$ of magmatic CO_2 in the French Lake Pavin (Aeschbach-Hertig *et al.*, 1999). In the French Massif Central, little is known on CO_2 emissions from the numerous carbogaseous springs that are part of the West European rift system, though several studies deal with the origin of such CO_2 (*e.g.* Batard *et al.*, 1982; Blavoux and Dazy, 1990; Czernochowski-Lauriol *et al.*, 2003). Only a rough estimate of the CO_2 emissions associated with quiescent volcanism in the French Massif Central is reported by Mörner and Etiope (2002) – citing Hermansson *et al.* (1991) – as being over 6 $kg.m^{-2}.y^{-1}$. And only one study quantified the CO_2 emissions into the atmosphere at the Sainte-Marguerite site (Battani *et al.*, 2010).

The present study thus aimed at quantifying the gas emissions related to quiescent volcanism in the French Massif Central near Lake Pavin (France *et al.*, 2016). Here, the CO_2 percolation is not associated with mineral water, thus leading to the appearance of mofette structures (CO_2 dry-gas vents), such structures commonly being related to Cenozoic rifting (Pearce *et al.*, 2004). In Europe, dry CO_2 vents occur, *e.g.*, in the Pannonian basin (Bräuer *et al.*, 2016), in the Eger rift zone (Kämpf *et al.*, 2013), in the Eifel volcanic district (Gal *et al.*, 2011; Krüger *et al.*, 2011). A large number is reported from Italy, though gas vents there can

93 be related to both magmatic CO_2 emissions and emissions of CO_2 accumulated in carbonated
94 reservoirs (Rogie *et al.*, 2000; Chiodini *et al.*, 2007; Beaubien *et al.*, 2008; Roberts *et al.*,
95 2011). In the French Massif Central, the only occurrence reported so far is the Escarot
96 mofette (Gal and Gadalia, 2011; Braüer *et al.*, 2017).

97 Our new investigations around this mofette used the complementary approaches of
98 measuring soil-gas concentrations (*e.g.* Fleischer and Mogro-Campero, 1978; Toutain and
99 Baubron, 1999) and soil-gas flux (*e.g.* Chiodini *et al.*, 1998). The data were used to quantify
100 the range of annual CO_2 emissions, to evaluate their relationship with geological structures
101 and to evaluate their contribution to the long-term global carbon cycle (*e.g.* Werner and
102 Brantley, 2003). Another part of the study was the assessment of changes in gas-emission
103 rates linked to the occurrence of major precipitation events, as fieldwork cannot always be
104 done under favourable weather conditions. Finally, we envisaged the consequences such gas
105 emissions may have in more populated areas.

106

107 ## 2. Settings

108 ### 2.1. Hydro(geo)logical setting

109 The study area is located 2 kilometres west of Lake Pavin, a maar lake characterized by its
110 meromictic character (Meybeck, 2015) that was formed around 7,000 years ago. The
111 volcanic system today is non-active, though some magma may still be present at depth
112 (France *et al.*, 2016). Compared to the duration of volcanic rest periods in the neighbouring
113 Chaîne des Puys (10,000 years or more), the system must be seen as quiescent (or dormant),
114 but not extinct. The dissolved CO_2 in the lake water is attributed to organic-matter
115 degradation (70% of total input) and to seepage of magmatic CO_2 and/or CO_2 from

116 methanogenesis (Jézéquel, 2015). Deep-CO_2 input becomes dominant in the deeper part of
117 the lake (Aeschbach-Hertig *et al.*, 1999). The presence of magmatic CO_2 from the sub-
118 continental lithospheric mantle was reported from the Fontaine Goyon mineral spring and
119 the Escarot mofette (Bräuer *et al.*, 2016, 2017). Meybeck (2015) reports that other degassing
120 spots seem to have been identified in the past.

121 The study area is small (about 200x300 m) close to the Escarot degassing zone (*Figure 1*).
122 The Escarot site was earlier described by Gal and Gadalia (2011) and by Bräuer *et al.* (2017).
123 A distinction has to be made between the location of the mofette as defined in 2011 (*Figure*
124 *1*) and the location of the data reported by Bräuer *et al.* (2017) that concerned samples
125 mostly taken around the Escarot piezometer (*Figure 1*). This observation well is part of a
126 network of several boreholes that were drilled in the late 2000s to resolve a controversy
127 about potential renewal of degassing activity (Meybeck, 2015).

128 The gas phase released at Escarot is dominated by CO_2 (>99.2% vol.) with a minor proportion
129 of permanent gases (N_2 <0.65%; O_2 <0.09%; Ar <0.007%) and traces of CH_4 (360 to 500 ppm)
130 and of He (27 to 30 ppm; Bräuer *et al.*, 2017). Higher helium concentrations in soil gas, up to
131 47 ppm were reported by Gal and Gadalia (2011). Isotope data on CO_2 ($\delta^{13}C_{CO2}$), from the
132 piezometer or the mofette (*Figure 1*), fall in a narrow range (-3.6 to -3.8‰ VPDB, Bräuer *et*
133 *al.*, 2017; -3.1 to -4‰, unpublished BRGM data) and so do the $^3He/^4He$ ratios (6 to 6.3 R/Ra,
134 Bräuer *et al.*, 2017; 6.09 R/Ra, BRGM unpublished data). Similar values are reported
135 regionally for magmatic CO_2 (*e.g.* Battani *et al.*, 2010; Gal *et al.*, 2017).

136 The new data were mostly acquired to the west of a road near the Escarot piezometer; here,
137 the ground level is approximately 3 m below the road and flooding occurs frequently. Near
138 the Escarot mofette, the ground level is approximately 2 m above the road. Several zones of

bubbling exist along the road and can be seen each time there is some stagnant water in the road shoulders (after precipitation events). As will be described later, these areas, which are frequently flooded, were investigated at the start of the fieldwork and were not accessible after large precipitation events. To the east of the road, there is a large area of peat land, where flux measurements were made on only unflooded clumps of grass as the soil is nearly saturated all year long. To the south of the monitoring area lie some meadows, but they, too, were almost saturated with water on the day they were investigated.

Figure 1

2.2. Methods

In June 2017, 44 soil-gas concentration measurements and 176 soil-gas flux measurements were made in the 200x300 m area (*Figure 1*). The objective was to obtain a more detailed description of the degassing area that was highlighted by 53 earlier soil-gas concentration measurements over a 250x400 m area (Gal and Gadalia, 2011). The new sampling aimed at lowering the uncertainty in the estimate of CO_2 emissions from the Escarot area (Werner *et al.*, 2000). As emissions of chemical species into the atmosphere from mofette structures are not restricted to just the gas phases, complementary data on soil gas and dissolved elements in snow cover, acquired in February 2009, are presented as Supplementary Material.

In order to reduce the uncertainty in soil-gas flux evaluations caused by the use of relatively small flux chambers (Parkin and Venterea, 2010), we used a 10-m-square grid close to the mofette and a 25-m-square grid farther away from the mofette (*Figure 1*). Flux measurements were done first, followed by soil-gas concentration measurements if

warranted by the flux results. Such soil-gas concentration measuring points were shifted 20 cm away from the flux chamber, to avoid wrong estimates on later flux acquisitions at the same location. All sampling points were marked in the field so that a repeat acquisition could be done in exactly the same place; in addition, the trace of the flux chamber often remains visible.

Soil-gas concentrations were measured with the same method as used before (Gal and Gadalia, 2011). Small holes (1 cm diameter) were drilled down to 1 m depth, and then a sampling probe was inserted that was plugged into an Infra-Red Gas Analyser equipped with a moisture filter (LFG20, ADC Gas Analysis Ltd., UK). Pumping was at a low flow rate of 200 $ml.min^{-1}$. Steady-state conditions were reached within tens of seconds. No concentration changes over a few minutes were noted. CO_2 and O_2 concentrations were directly monitored. The monitoring of CH_4 concentrations was not technically feasible (detection limit of 200 ppm at best), but the Escarot mofette is not CH_4-rich (Bräuer *et al.*, 2017). Analytical precision for CO_2 was ±0.5% of the reading for low concentrations (0.01–10% vol.), ±3% of the reading for higher concentrations (10 to 50% vol.) and ±5% of the reading when CO_2 was >50%. The precision for oxygen was ±0.4% of the full scale reading (0–25% vol.). Samples were stored in Tedlar® bags and analysed by the end of the day for ^4He with mass spectrometry (Adixen ASM102S leak detector, France) with reference to atmospheric content (5.24 ppm). Precision of the measurement was better than 4% at full scale.

Soil-gas flux measurements used the accumulation chamber method with external recirculation (*e.g.* Chiodini *et al.*, 1998; Inguaggiato *et al.*, 2013). The flux-chamber system was a customized version of the Echo Instruments (Slovenia) soil-gas flux system. The

aluminium chamber has a semi-spherical shape with a basal area of 0.0289 m^2 and a volume of 0.0018 m^3-(soft ground). The chamber was directly put on the soil surface, which is mainly grassland with some gravel patches close to the road. No soil was removed except incase (point C9). A fan with variable speed ensured the mixing of the headspace gas as required for such sampling (Parkin and Venterea, 2010). The flow rate of the recirculation flux was set to 0.5-0.6 $l.min^{-1}$, to avoid possible underestimations of the CO_2 flux when lower recirculation flow rates are used, as well as to avoid possible CO_2 flux overestimations when using higher recirculation flow rates (Camarda *et al.*, 2009). Pressure, temperature and relative humidity inside the chamber, as well as pumping rate, were continuously monitored thus constraining the possible influence of external parameters on the data. The following gas species were monitored after the gas passed through a moisture filter: CO_2 and CH_4 by Non-Dispersive Infra-Red (NDIR) detectors (0 to 5000 ppmv ±2% and 0 to 10000 ppmv ±5%, respectively), and O_2 by electrochemical cells (0 to 25% vol. ±2% of the reading).

Some examples of field-data acquisitions are given in *Figure 2*. The flux calculation was based on the rate of CO_2 increase (positive flux; *e.g.* point A15, *Figure 2*) and potential O_2 decrease in the chamber (*e.g.* points BZ8, E12, *Figure 2*). The flux was calculated by considering the linear build-up of gas concentration in the chamber during 3 minutes and by determining the initial slope of the gas-concentration *vs*. time relationship (*e.g.* Chiodini *et al.*, 1998; Werner *et al.*, 2000). Flux was normalized to take into account the influence of pressure and temperature (Lewicki *et al.*, 2005). Normalized CO_2 flux generally was 4.5% higher than raw flux values.

Not all fluxes were calculated using the initial slope of the build-up of gas concentrations. Short time-scale variations of the CO_2 flux (gas flush) were sometimes observed (*Figure 2*)

and were used to evaluate the uncertainty on the gas release. Increases of 10 times of the flux over some seconds were noticed in points A8 (once) and Z16 (several times). Such multi-linear increases were also reported from the Yellowstone area (Werner *et al.*, 2000).

Figure 2

2.3. Weather parameters

It is well established that soil-gas concentrations and fluxes can be affected by, among others, meteorological parameters such as temperature, atmospheric pressure, wind or precipitation (*e.g.* Hinkle, 1994; Toutain and Baubron, 1999; Viveiros *et al.*, 2008, 2009; Werner *et al.*, 2014). Unexpectedly for late June, the weather was strongly variable. No precipitation was reported during the week preceding fieldwork at a nearby weather station (*Figure 3*). Air temperatures were quite high and pressure showed little variability. The situation changed the weekend before the fieldwork. Temperature and pressure steadily fell between 24 and 29 June, and large precipitation events occurred during late afternoon on 26 and 27 June (31 mm and 34.6 mm, respectively). June 28th and 29th were rainy days, with intermittent precipitation events on the 28th (10.8 mm) and continuous precipitation events on the 29th (14.8 mm).

The gas-concentration and -flux dataset was acquired as follows: 45 flux measurements prior the rainfall (26 June), 56 flux and 22 concentration measurements after 31 mm of rain on 27 June, 42 flux and 15 concentration measurements after >65.6 mm of precipitation on 28 June, and 33 flux and 7 concentration measurements after >76.4 mm of rain on 29 June.

The temperature and pressure data recorded during flux acquisitions are in good agreement with the weather station data (*Figure 3*). Temperature during the first two days rose during the day as a consequence of sunshine thermal forcing, the humidity of the gas at the soil/atmosphere interface thus decreasing during the day. During the last two days, the situation was reversed as there was no sunshine; the soil-gas humidity was high and further rose during the day after the rain.

Because of these large precipitation events, there was a strong correlation between temperature and pressure (Pearson's coefficient of 0.88), relative humidity and temperature of the atmosphere (coefficient of -0.89), and relative air humidity and atmospheric pressure (coefficient of -0.82) during flux measurements.

Figure 3

3. Results and discussion

3.1. Statistical parameters

The main statistical characteristics of the soil-gas concentrations and fluxes measured in 2017 are shown on *Figure 4*. Former concentration data measured near the Escarot mofette, between 2008 and 2012, are also shown; the location of these data is shown on the bottom map of *Figure 1*.

As may be expected from a survey designed for highlighting the behaviour of soil-gas species near a gas vent, the data distribution of soil-gas concentrations shows a very high mean CO_2 concentration (72.6±36.1% – arithmetic mean ± standard deviation), a very low mean O_2 concentration (5.8±6.8%) and a strong enrichment in helium-4 in the soil (19.9±13 ppm as a

mean). By comparison, data from the 2008 to 2012 surveys in the Escarot area showed mean CO_2 and helium enrichments (47.3±43.7% and 17.3±9.6 ppm, respectively) and O_2 depletion (11.1±8.5% as a mean), suggesting that the degassing pattern of the Escarot area has remained stable over several years.

No CH_4-flux was measured during the survey, but this is not really surprising. Even on active volcanoes, the diffuse CH_4 flux may only represent trace releases compared to diffuse CO_2 degassing (Hernández *et al.*, 1998).

As the variation coefficient of CO_2 flux shows a skewed distribution, which is common in high-flux areas, we refer to the arithmetic mean as explained by Werner and Brantley (2003) and references therein. Three evaluations are presented in *Figure 4*. The first corresponds to the data calculated using the linear fit prevailing during most of the sampling and considering the normalization to standard temperature and pressure (STP) conditions. The second evaluation corresponds to the flux calculated from the gas flush(es) that may occur along the 3-minute-long flux acquisition (*Figure 2*), called “maximum value”. The third evaluation combines the previous two datasets in order to account for the short-term variability induced by the occurrence of gas flushes. The STP values are thus corrected to include these potential short-term increases, the “maximum value” being integrated as a function of the number and duration of the increases observed during the acquisition. The ponderated flux value deriving from this last calculation thus represents the best estimate of the gas emission over 3 minutes.

Such gas flushes can have a noticeable influence: they were observed for 59 of the 176 acquisitions. The minimum duration of a gas flush over 3 minutes was 5 seconds (one event) and the maximum was 75 seconds (several events of up to 15 seconds duration each).

Maximum fluxes that may be calculated during these short events are shown at least by an increase of 20% of STP-flux, a value similar to the error reported for flux measurements (±15%; Chiodini *et al.*, 1996). At most, the increase corresponds to a multiplication by a factor of 20 of the flux. As a mean, gas flushes induced a short-term increase of the flux by a factor of 7 (*e.g.* for point A8, *Figure 2*). Only few points showed a decrease in CO_2 flux during the acquisition (*e.g.* point Z32, *Figure 2*), which can lower the flux by up to 40% and is only noted at low emissive points. Consequently, the initial mean value of the uncorrected STP-flux data (500±2,080 $g.m^{-2}.d^{-1}$) is re-evaluated at 575±2,100 $g.m^{-2}.d^{-1}$ (*Figure 4*).

Figure 4

3.2. Data analysis

3.2.1. Relations between gas species

The CO_2-O_2 relationship for soil gas is presented in *Figure 5A* and interpreted using the process-based approach of Romanak *et al.* (2012). Three main relationships are plotted. The first is the respiration line (in blue), characteristic of aerobic respiration in soil that consumes 1 mole of O_2 to produce 1 mole of CO_2. The second relation corresponds to the CH_4 oxidation line (in green) in near-surface environments, where 2 moles of O_2 are needed to produce CO_2+H_2O. The last relationship (red lines) corresponds to the dilution process occurring when a deep (magmatic) CO_2 endmember dilutes the O_2+N_2 pool in a near-surface environment (relative abundance: 20.9% of O_2 and 78.1% of N_2). Different dilution lines can be plotted, depending on the CO_2/O_2 initial ratio: *Figure 5* illustrates three cases at 0.03%, 5% and 10% of biologically produced CO_2.

Only few data lie on the respiration line and these have a CO_2 concentration below 5%. Most of the data plot close to the dilution line with a possible influence of respiration processes. This kind of data distribution confirms previous data that reported a threshold value around 10% of CO_2 in soil (Gal and Gadalia, 2011). Below this value, CO_2 mainly originates from biological processes; above it, a supply of deep-seated CO_2 is required. The area investigated around the Escarot mofette (*Figure 1*) is thus largely influenced by the degassing of magmatic CO_2, as shown by the general relationship between CO_2 and O_2 concentrations (slope of -0.20). Biological processes, though existing, have little influence on the relation between these two gas species.

Strong helium enrichment (>10 ppm) was earlier measured when the CO_2 concentrations were over 10% (Gal and Gadalia, 2011). *Figure 5B* links ^{4}He data to CO_2 data and similar conclusions arise from the ^{4}He-O_2 relationship in the present study. In 2017, there still was a good correlation between ^{4}He and CO_2 as shown by the overlapping fits in *Figure 5B*, even if the helium enrichment of soil gas seems to be lower in 2017 for CO_2 concentrations below 80%. However, for a nearly pure CO_2 gas phase, ^{4}He concentrations were higher than previously measured. Despite a less sensitive character, the new data still suggest that helium is a good proxy for detecting the presence of deep-seated CO_2.

The variability of the helium signal in soil gas may have at least three different origins. First, it may have been a result of the poor weather conditions during the 2017 fieldwork, with their potential impact on pressure and temperature gradients in soil that govern advective transport (*e.g.* Werner *et al.*, 2000; Etiope and Martinelli, 2002; Rinaldi *et al.*, 2012). Second, such variability may be caused by demixtion phenomena that are variable over time (Gal and

317 Gadalia, 2011). Third, such variability in the helium signal this may also be caused by long-
318 term variability of the deep-seated gas efflux (*e.g*. Chiodini *et al*., 2010; Werner *et al*., 2014).

319 Finally, our data show a good correlation between CO_2 flux and O_2 depletion. *Figure 5C*
320 presents this relation with reference to the domain of biological CO_2 efflux as recently
321 established in France by Pokryszka *et al*. (2017). The maximum efflux mentioned by these
322 authors is close to 84 $g.m^{-2}.d^{-1}$ (or 30 $cm^3.min^{-1}.m^{-2}$) for summer acquisitions and close to
323 34 $g.m^{-2}.d^{-1}$ (or 12 $cm^3.min^{-1}.m^{-2}$) for winter acquisitions, the last value being closer to
324 maximum values for biogenic flux reported in other areas (*e.g*. Werner and Brantley, 2003:
325 30 $g.m^{-2}.d^{-1}$). Any CO_2 flux over 84 $g.m^{-2}.d^{-1}$ strongly suggests a relation with deep-seated
326 processes. *Figure 5C* shows a fairly good relationship between the CO_2 flux and O_2 depletion,
327 with large depletions associated with strong emission of CO_2 into the atmosphere. This is the
328 translation on the flux parameter of the flush effect existing for soil-gas concentrations, this
329 effect being induced by the intrusion of deep CO_2 in the soil that sweeps away the naturally
330 existing O_2+N_2 pool in soil. When the strength of the CO_2 efflux is high, then the sweeping of
331 O_2 can also be monitored using the depletion of O_2 concentrations at the soil/atmosphere
332 interface. Such monitoring may be an interesting – and complementary – tool for testing the
333 strength of deep-seated gas emissions.

334 Correlation-matrix calculation fails to suggest the existence of other relations between the
335 different gas phases. It is nonetheless important to assess if CO_2 flux is related to CO_2 or ^4He
336 soil-gas concentrations, markers of deep-seated processes in the present case (*Figure 6*).
337 Four groups are defined in *Figure 6A*. Group A has typical CO_2-flux values overlapping the
338 ones of biological sources, though the CO_2 concentrations may be much higher than those of
339 biologically produced CO_2 in soil gas. Group B marks a clear departure from this biological

pool, especially when considering the high CO_2 concentration values, and group C is only related to CO_2 leaks from depth. There is a graphical trend from Group A to Group C, which suggests that the higher the CO_2 concentration, the higher will be the CO_2 flux. Group D corresponds to high CO_2 concentration in the soil, but low flux at the surface. *Figure 6*B shows that this 'low CO_2 flux' group is He-rich too, suggesting that the soil structure has an influence on gas emission to the surface (June 26th acquisitions) and that an additional influence of precipitation may be invoked for acquisitions made on June 27th.

The difficulty of monitoring low fluxes over soils that only have CO_2 as a soil-gas phase may be linked to several reasons. One reason is the presence of variable amounts of clay in the soil in the area (*Figure 7*). Because of changing weather conditions and large precipitation events, the upper part of the soil can reach near-saturation conditions (low CO_2 flux), but at 1-m depth the soil may allow efficient gas advection. Another reason may be the distance from the main CO_2 supplying areas, *i.e.* from highly permeable fault zones. Above a degassing structure, high flux and high CO_2 concentrations are supposed to occur conjointly (Gal *et al.*, 2011, 2012, and references therein), but at some distance of such structures, the strength of advection processes may be lower, thus lowering the efflux at the soil/atmosphere interface.

This reasoning can be extended to the helium concentrations in soil gas. Tendency (1) in *Figure 6B* is found close to or above a deep-rooted degassing structure where a strong ascent of gas causes combined strong CO_2 and ^{4}He enrichment (>30 ppm). Nonetheless, as highlighted by Tendency (2), the higher ^{4}He values in soil are not found in high CO_2 flux zones (*i.e.* they are found with some distance to the degassing structures), but they correspond to 100% of CO_2 in the soil. In that case, soil permeability may play a role even if some authors

363 consider permeability to be of secondary importance (Camarda *et al.*, 2006). More precisely,
364 the presence of water in the upper part of the soil may be the cause. If the first 10-20 cm are
365 saturated after precipitation, then the emissivity of the soil will be low (low CO_2 flux), but
366 farther down in the soil, the soil-gas concentrations can be high: the data shown on *Figure 4*
367 suggest that high CO_2 concentrations are widespread at the scale of the Escarot site so that
368 having 100% CO_2 in soil gas is a common phenomenon. Helium has a larger diffusive capacity
369 than CO_2 (*e.g.* Jähne *et al.*, 1987), as well as a much lower solubility in water (*e.g.* Weiss,
370 1971, 1974). If a saturated horizon is present in the upper part of the soil, then the barrier
371 effect ("soil capping", Werner *et al.*, 2000) induced by this horizon may not be noticed when
372 considering CO_2 concentrations (high background), but it may cause an increase in ^4He
373 concentration as the leaking of helium to the atmosphere is considerably reduced because
374 of the presence of a water-saturated horizon. Lateral diffusion of ^4He may also contribute to
375 local enrichment.

376 Figure 5

377 Figure 6

378

379 **3.2.2. <u>Relationship with meteorological parameters</u>**

380 *Figure 3* illustrates the changing weather conditions during sampling. This offered an
381 opportunity further to evaluate the influence these parameters may have on flux
382 quantification, even it is preferred to sample soil gases during periods of dry weather.
383 Correlation-matrix calculations highlight a good correspondence between the changes in
384 temperature and relative humidity (Pearson's coefficient of correlation r of -0.887), of

385 temperature and pressure (r of +0.876), and thus of pressure and relative humidity (r of -
386 0.816). The amounts of precipitation also negatively correlated with the relative humidity (r
387 of -0.830). Huge amounts of rain fell during the strong precipitation events, increasing the
388 humidity at the soil/atmosphere interface. By the end of the sampling period, the amount of
389 precipitation was much lower, but the cumulative amount was high and thus the rise of
390 relative humidity continued. Nonetheless, these calculations fail to illustrate if there is a
391 global influence of these meteorological parameters onto the soil-gas and soil-flux data. For
392 instance, correlation coefficients are <0.1 (r) when comparing CO_2-flux data with
393 temperature, pressure or relative humidity. This suggests that external parameters exert
394 little to insignificant influence on degassing processes; this is congruent with a deep-seated
395 origin of the gases and with the low variability of the degassing strength that is expected for
396 a monitoring period of short duration (*e.g.* Werner *et al.*, 2014).

397 However, it is well established that external parameters can have a strong influence on the
398 acquisitions (*e.g.* Oertel *et al.*, 2016), and especially on flux data when considering the
399 duration of our survey. A time span of three days may be too short to allow the percolation
400 of water to 1-m depth, particularly during summer when water is easily taken up by the
401 vegetation. For instance, Werner *et al.* (2014) report a decrease of emission rates by a factor
402 of 2-3 over several days after the passage of a weather front associated with high winds and
403 strong precipitation: they highlight the influence of wind in this decrease as this may change
404 the pressure gradient in soil. This may be less obvious for our dataset because the wind
405 speed measured during the survey (maximum 3.33 $m.s^{-1}$) and far below the 14 $m.s^{-1}$ reported
406 by Werner *et al.* (2014). As temperature, pressure, amount of precipitation and relative
407 humidity are interdependent, it is not easy to designate the most influent parameter, though
408 rain and its consequences on soil moisture are of primary importance (*e.g.* Viveiros *et al.*,

2014, and references therein). We will thus use the generic term “precipitation event” to describe the influence of external parameters on flux evaluation.

Some examples are shown in *Figure 7* to illustrate different aspects. Short-term variations under consistent weather conditions were assessed through repeat acquisitions at points Z13, Z18 and Z19 before precipitation events (grey and blue dots on *Figure 7*) and at point E12 after several precipitation events, in order to evaluate the bias that may exist for high CO_2 fluxes. Under dry weather conditions, the variability in CO_2 flux was between 2.5% and 12% for points showing similar degassing properties (points Z13 and Z18). This 2.5-12% variability is in reasonable agreement with the standard error of this method (*e.g.* Chiodini *et al.*, 1996; Evans *et al.*, 2001). This is also similar to what is reported for the amplitude of flux variation even under stable weather conditions (10% to 20%; Viveiros *et al.*, 2014). The variability can be much higher when gas flushes exist (300% of variability for point Z19). High intrinsic variability may thus be caused by these flushes of unpredictable variability, which were common during our acquisitions and represent fluctuations of the advective component (Werner *et al.*, 2000). For point E12, the reduction of flux was around 150% and associated with increased soil moisture, but no acquisition was done before precipitation events so that the decrease between dry and wet conditions may be much larger.

The occurrence of a precipitation event may not always points to a decrease in CO_2 flux. An increase of the flux was monitored at point Z13 after the first precipitation event (*Figure 7*). As shown on the three photographs above the plot, the area of point Z13 was bare and the soil was humid (31 mm precipitation, evening of 26 June). Surprisingly, this had no influence on the gas emission as the flux was 25% higher. This is certainly due to the location of this point Z13, as shown by the strong bubbling on 28 June after another large precipitation

event. The monitoring point was just above a degassing centre and soil saturation had almost no influence on this process at least over a short period. Though not frequent, such an increase of gas flux after rainfall may also occur in areas where water taken up by the vegetation, such as point EZ12. General flux was low, in the range of biological CO_2 flux (Pokryszka et al, 2017), but an increase of +60% was measured after the second precipitation event. Some of this variability may also be linked to the daily variability of biological soil-gas efflux (*e.g.* Parkin and Kaspar, 2003).

Normally, flux (*e.g.* Werner *et al.*, 2000) and soil-gas concentrations (*e.g.* Hinkle, 1994) decrease after precipitation events. This is illustrated for flux by repeat acquisitions at points CZ4, Z18 and Z19 (*Figure 7*); a decrease by a factor 5 or 10 occurred after 31 mm of rain (respectively, points Z18 and Z19). Werner *et al.* (2000) reported a decrease by a factor 2 after 21 mm rain in the Yellowstone area. Further decrease may occur as the cumulative precipitation increases (-15% at Z18, 8-fold decrease at CZ4). Such huge decreases are the direct result of soil capping, which is maximized when acquisitions occur during precipitation events. It is thus recommended to wait for two days without any precipitation to get rid of the potential effects of water saturation in the soil pores (*e.g.* Fridriksson *et al.*, 2006), but this was not possible during our survey.

Soil properties must be considered as well. In volcanic areas, high degassing zones are generally located on or near faults, meaning that soil permeability will have only minor influence on flux values (Camarda *et al.*, 2006), and a shallow soil cover may only slightly affect the shape and size of the soil degassing anomalies. However, this general statement has to be verified for each study (Viveiros *et al.*, 2014), and in our case the influence of the soil cover is shown by the increase in CO_2 flux at point C9 (*Figure 7*). Here, a first direct measurement was followed by the removal of the uppermost few centimetres; the second

456 measurement, 15 minutes after the first, then showed a 6-fold increase in CO_2 flux. This
457 delay may be too short to reach stability of the gas efflux; Fridriksson *et al.* (2006) indeed
458 mentioned a duration of 30 minutes to reach steady-state conditions. Nevertheless, the
459 amplitude of the increase also suggests that the clayey topsoil strongly reduced the gas
460 emission, especially when rain fell before the acquisitions. This may explain some of the
461 discrepancies between soil-gas concentrations and soil-gas flux, the second being far more
462 affected by the humidity and type of soil. There may be exceptions to this rule as shown by
463 the data from point E12, which is close to a road on gravel banks that are highly permeable
464 even under wet conditions. Some variability (40%) was noted between repeat acquisitions,
465 but this was largely due to uncertainty on the rate of CO_2 enrichment in the chamber in the
466 case of very high emissions.

467 Precipitation events were common during this survey, more or less affecting three quarters
468 of the acquisitions. Direct use of these field acquisitions to calculate the CO_2 budget into the
469 atmosphere would probably underestimate this budget. We thus corrected the dataset to
470 arrive at a better assessment of the gas emissions, based on relationships established
471 between the data points that were measured before and after precipitation events.

472 Based on the above-described data, this underestimate can be evaluated at up to 500% for a
473 flux range of 96-720 $g.m^{-2}.d^{-1}$ just after a large precipitation event, whereas higher fluxes
474 (>1440-1920 $g.m^{-2}.d^{-1}$) that are found in areas with potential bubbling manifestations are not
475 really modified. When precipitation events are less intense but last for several hours, an
476 additional drop of the flux by approximately 15% is seen. We thus propose the following
477 empirical correction procedure: 1) 45 data from 26 June: no correction; 2) Data from 27
478 June: if CO_2 flux is <240 $g.m^{-2}.d^{-1}$ the value is multiplied by 5 (49 data); if the flux is 240 to

1440 g.m^{-2}.d^{-1} the value is multiplied by 2 (5 data); if CO_2 flux >1440 g.m^{-2}.d^{-1} there is no correction (2 data); 3) Data from 28 and 29 June: similar correction as for 27 June data and an additional correction of +15% (multiplied by 5 +15%: 28 data; multiplied by 2 +15%: 2 data; no correction: 3 data). Data corrected only for pressure and temperature effects and those including further correction steps (gas flush and precipitation events) are compared in *Figure 8* (data shown in Supplementary table). The effect of this correction procedure is greatest for low fluxes considered as extreme. Some low CO_2 flux values after precipitation correction are still less than 40 g.m^{-2}.d^{-1}, but most are much higher and point to CO_2 flux values far above biological ones. Even if this procedure likely represents an over-correction of the data, it should still be used when evaluating CO_2 release at site scale, to give a range indication of the maximum expected gas release.

Figure 7

Figure 8

3.3. Spatial distribution

3.3.1. Background values and threshold levels

Soil-gas and soil-flux data are usually processed in order to determine threshold values from the data distribution. Such threshold levels help in better distinguishing between a pure biological, deep-seated, or mixed origin (*e.g.* Bloomberg *et al.*, 2014), using the procedure proposed by Sinclair (1974) that relies on probability plot calculations. This procedure may be adapted when the dataset is skewed, as is the case here with neither a normal nor log-

500 normal distribution, except for helium data that range under normal law with a p-value of
501 0.20. Some inflections in the cumulative probability plot may exist (*Figure 9*).

502 In our case, the acquisitions were oriented towards definition of the mofette structure and
503 not towards a characterization of the background population, which may correspond to soil-
504 respired CO_2 emissions. Nevertheless, an upper limit for biologically sourced CO_2 in the soil,
505 close to 10% may be deduced from the 2017 CO_2 data (blue on *Figure 9*) and from the
506 previous dataset (red on *Figure 9*). A similar result derives from the earlier described CO_2-O_2
507 relationship. An upper threshold of 80-90% CO_2 may be defined, but its sole significance is to
508 help locating potential gas vents that show strong emission into the atmosphere as a
509 function of meteorological and soil parameters.

510 The helium data showed a similar distribution in 2017 (Escarot area) and in 2008-2012 (over
511 a much larger area), suggesting some representativeness. A lower threshold of 5.5 ppm can
512 be defined and corresponds to near-atmospheric values accounting for a measuring error of
513 5% (5.24 x 1.05 = 5.5). The upper threshold is around 24 ppm and any value above this
514 threshold will indicate the presence of deep-seated gas phases.

515 Finally, depending on which CO_2 flux data are considered (*Figure 9*), the biological
516 background value can range from <33.6 $g.m^{-2}.d^{-1}$ (precipitation correction taken into
517 account) to <74.4 $g.m^{-2}.d^{-1}$ (data normalized to STP conditions). The higher value is close to
518 the upper limit defined by Pokryszka *et al.* (2017) for French soils. Higher flux values are
519 typical of strong gas emissions with a growing influence of deep-seated CO_2 feeding. Mixed
520 sources (biological and deep-seated) may exist until the 240 $g.m^{-2}.d^{-1}$ threshold level is
521 reached.

522 Figure 9

523

524 ### 3.3.2. Data interpolation

525 As may be expected from the skewed data that were acquired near the gas seeps, all gas
526 data show an anisotropic behaviour as pointed out by variogram calculations. Variograms for
527 soil-gas data (data not shown) are best fitted using a preferential distribution along a N60°
528 axis, whereas soil-gas flux data rather show a preferential distribution along a N25° axis. The
529 lag distances were calculated between 50 and 60 m except for helium (35 m). This agrees
530 with the size of emitting areas reported elsewhere for CO_2 or CH_4 degassing structures (*e.g.*
531 Battani *et al.*, 2010; Etiope *et al.*, 2010). These data were used to construct interpolated
532 maps for an area of about 310 m N-S by 170 m E-W.

533 The interpolated maps for CO_2 flux and correlative O_2 depletion (*Figure 10A and B*) show
534 several degassing centres that seem to be aligned along a roughly NNW-SSE direction.
535 Several seeps of secondary degassing power occur in the north of the area, between the
536 piezometer and the first mofette centre (as defined by Gal and Gadalia, 2011), releasing
537 2,400 to 3,600 $g.m^{-2}.d^{-1}$ of CO_2 into the atmosphere. Interestingly, this NNW-SSE direction is
538 also revealed by O_2 depletion data at the soil/atmosphere interface, indicating the most
539 efficient degassing centres. Two main such centres are located in the south of the area. The
540 less emissive one releases about 6,000 $g.m^{-2}.d^{-1}$ of CO_2, whereas the most active can reach
541 over 14,000 $g.m^{-2}.d^{-1}$ of CO_2 (Point E12, *Figure 7*). This most active area, set close to the road
542 over a gravel bed, shows no traces in the vegetation (grass) that might suggest the existence
543 of such strong CO_2 release. Compared, *e.g*, to the Latera gas vents, of lower release strength
544 (2,000 to 3,000 $g.m^{-2}.d^{-1}$; Beaubien *et al.*, 2008) but without vegetation, the absence of
545 visible effects at Escarot is probably related to the absence of reducing gas species such as

546 H_2S or CH_4, which are released at Latera. Based on the maps constructed from STP-
547 normalized flux or that corrected for precipitation effects, an inner structuring of these high
548 release seeps seems to exist. This potential structure is oriented NE-SW, but, as the map
549 built using the flux accounting from gas flushes does not reveal the same secondary
550 structuring, this may be an artefact from kriging calculations and thus little confidence is
551 given to this feature.

552 The soil-gas concentration measurements shown on *Figure 10C* include all the available
553 (2008-2012 and 2017) data. The resulting interpolated maps show a good spatial agreement
554 between these data, as was expected from probability-plot results (*Figure 9*). The data
555 define several structures in the soil where CO_2 and ^4He enrichment and the correlative O_2
556 depletion may be very high. The mofette and the piezometer are located on two of these
557 structures that are also aligned along a NNW-SSE direction. Helium enrichment appears to
558 be less important to the southeast, but this effect may be caused by a lack of data is this
559 area.

560 At site scale, the soil-gas and soil flux measurements correlate. Areas where CO_2 flux is high
561 are rich in CO_2 in the soil, but not all areas rich in CO_2 in the soil show high CO_2 release into
562 the atmosphere. Similar spatial correlations were reported by Battani *et al.* (2010) and
563 highlight the role of soil in the shape and size of degassing (Camarda *et al.*, 2006).

564 The structure and surface arrangement of degassing centres perfectly match the known
565 regional tectonic structures. Brousse *et al.* (1990) reported the existence of NE-SW to NNE-
566 SSW faults whose directions were inherited from pre-existing fractures in the Hercynian
567 basement. Locally, these authors also mention the existence of a recent NNW-SSE fault
568 (*Figure 10B*) that separates two series of the Mont-Dore volcanism (3 to 1.2 Ma-old basalt to

the west and 1.2 to 0.3 Ma-old benmoreite to the east). Hydrothermal traces exist along this fault over some tens of metres across the fault trace. This fault becomes invisible about 300 m north of the Escarot piezometer after offsetting the surficial formations filling the valley. Farther south this fault has no surface expression, but our data show that its trace can be extended as it still has some permeability for gas phases.

Figure 10

3.4. Quantifying gas release to the atmosphere

The strength of degassing and thus the permeability of the fault to gas flow can be assessed using the interpolated maps described above *(Figure 10)*. Such evaluation is based on volume calculations functionalities that are found in *e.g.* Surfer software (Goldensoftware), provided the coordinates are in metric scale (*e.g.* Werner *et al.*, 2000). *Table 1* shows some results.

The CO_2 that is released into the atmosphere may not all be of deep-seated origin (*Figure 5*). Three different levels of background biological flux are considered: 30 $g.m^{-2}.d^{-1}$, the common upper limit for biological flux; 48 $g.m^{-2}.d^{-1}$, the upper limit for grassland and agricultural soil; and 84 $g.m^{-2}.d^{-1}$, the upper limit reported for French soils. Each increase of the biological CO_2 flux induces a decrease of the deep-seated CO_2 component.

The first evaluation refers to the STP-normalized CO_2 flux, without considering any further correction. The second evaluation includes a correction to take gas flush into account. The third evaluation adds a correction to consider the effect of precipitation events, as earlier mentioned. Finally, a basic estimate is given, simply using the surface of the monitored area

591 (52,000 m^2) and the mean CO_2 flux (576 $g.m^{-2}.d^{-1}$). The end result is an emission of 30 tons
592 per day (tpd) of CO_2 into the atmosphere.

593 The first two evaluations gave quite similar results: the area affected by degassing is smaller
594 than 32,000 m^2 (60% of the investigated area) and larger than 17,000 m^2 (33% of the
595 investigated area). The amount of biologically produced CO_2 for a 52,000 m^2 area is between
596 1.6 and 4.4 tpd (depending on soil productivity). Interpolation calculations show that some
597 areas may not be as productive as expected, so the biological CO_2 flux was re-estimated at
598 between 0.7 and 2 tpd. This correction could only be a calculation bias linked to the
599 procedure itself, but it may also be representative: biological flux can naturally vary and may
600 be low in areas where deep CO_2 escapes. The resulting quantity of such deep-seated CO_2 is
601 evaluated between 17.3 and 20.8 tpd. The third evaluation, including the flux decrease
602 related to precipitation events, leads to quantities of emitted CO_2 very close to that of the
603 basic estimate (27 to 30 tpd), suggesting that even the most basic assumption can lead to a
604 realistic result, where the role of biological CO_2 flux is higher but nearly all the area appears
605 to be affected by diffuse degassing. This may be an optimistic appraisal, but we nevertheless
606 used it for proposing an overall estimate of the CO_2 budget, based on the mean value of all
607 estimates presented in *Table 1*. The CO_2 degassing over 0.052 km^2 at Escarot is thus
608 estimated at between 8100±1800 tons per year with an additional biological contribution of
609 660±400 tons per year, or respectively 22.2±4.9 and 1.8±1.1 tpd.

610 This amount of deep-seated CO_2 is three times larger than that reported regionally from
611 Sainte-Marguerite, 35 km to the north-east, where a CO_2 release of 8.5 tpd over 0.06 km^2
612 was estimated (Battani *et al.*, 2010). This quantity is similar to that emitted by diffuse
613 degassing in volcanic environments, such as in Greece (25 tpd, 0.346 km^2; Brombach *et al.*,

614 2001), in Italy (Stromboli Island: 20 tpd on the flanks; Inguaggiato *et al.*, 2013), in Japan
615 (74 tpd of hydrothermal CO_2 reported over 0.58 km^2 by Hernández-Perez *et al.*, 2003), or in
616 New-Zealand (Taupo Volcanic Zone: from 8±3 tpd over 0.3 km^2 to 72±13 tpd over 0.19 km^2;
617 Bloomberg *et al.*, 2014). Far higher emissions are nevertheless known from other volcanic
618 areas (*e.g.* Viveiros *et al.*, 2010; Burton *et al.*, 2013; and references therein) and also for
619 other mofettes in Europe (1566 tpd over 0.075 km^2 in the Czech Republic; Kämpf *et al.*,
620 2013).

621 Table 1

622

623 **3.5. Links to risk assessment**

624 The second aspect of this study relates to risk assessment, of interest to the populated areas
625 that exist a few dozen kilometres to the north-east. The Escarot area is not inhabited, but
626 cattle grazing close to, or over, the seep apparently is unaffected by the strong gas
627 emissions. However, this situation can be different when transposed to urban areas. Gas-
628 emission occurrences are known from the French Massif Central, especially in its capital city
629 Clermont-Ferrand, where some degassing spots release as much as 18 to 100 tons CO_2 per
630 year over 1 m^2 (Gal *et al.*, 2017). In an urban context, buildings and other constructions often
631 hamper and modify natural degassing pathways, thus focusing and/or enhancing the
632 release, possibly causing gas accumulations in foundations or cellars. For comparison, the
633 highest emission rate measured at Escarot leads to a release of 'only' 7.5 tons CO_2 per year
634 over 1 m^2. As a result, the population could be exposed to a gas hazard, but there may be no
635 warning signal, such as H_2S, in the gas phase or damage to the vegetation. The Escarot case
636 study can be seen as an analogy to the situation prevailing before human occupation. It

637 strongly suggests that further investigations are needed in (future) urban areas, to evaluate
638 the potential hazard and, if yes, to assess the composition and volume of gas releases, as is
639 done in Italy (*e.g.* Carapezza *et al.*, 2012).

640

641 **4. Concluding remarks**

642 With the aim of better evaluating emissions of non-anthropogenic gas and their influence on
643 the global carbon cycle, the 2017 fieldwork on the Escarot site revealed that CO_2 emissions
644 into the atmosphere are not of minor importance compared those reported from
645 volcanically more active environments. At ground level, a NNW-SSE elongated structure was
646 revealed, marked by several degassing centres that are located as a function of soil
647 properties and their relative permeability to gas transport. In the soil, the presence of CO_2 is
648 even more common, and a clear relationship with local and regional fault directions was
649 established. Local biological CO_2 production can be high (up to 10% of soil-gas), thus
650 contributing to a total mean CO_2 release into the atmosphere of 660 tons per year (tpy) for
651 the 52,000 m² area. This agrees with the magnitude of CO_2 emissions reported by
652 Hermansson *et al.* (1991), when extrapolated to a similar scale (310 tpy). The present case
653 highlights the need for better understanding the CO_2 emissions at the scale of the French
654 Massif Central, because existing evaluations may have missed far higher CO_2 emission rates
655 associated to mineral springs and/or gas vents. The existence of structures emitting CO_2 in
656 populated areas should also be taken into account in risk scenarios.

657 The deep-seated contribution is evaluated at over 8,000 tpy of CO_2 and compares well with
658 gas emissions reported for diffuse degassing in some active volcanic areas. However, gas
659 emissions may vary throughout the year, depending on the season and on meteorological

conditions. Very strong, though temporary, decreases of flux into the atmosphere (up to a factor 5) are caused by precipitation that saturates the upper soil horizons, and the presence of snow cover during winter may further reduce the yearly CO_2 budget. In addition, the rise of deep-seated CO_2 is not a linear process and high-frequency changes in gas-emission rates have been noted. The result is a quite high uncertainty as to the quantification of such gas emissions (±1,800 tpy), or about one quarter of the overall estimated amount of CO_2.

Acknowledgments

The authors would like to thank C. Werner and an anonymous reviewer for their thoughtful comments, which greatly improved this manuscript. The 2017 work was carried out with the financial assistance of the BRGM Laboratory Division (IN-SITU project). The previous work was part of a project funded by the Natural Risks Department of the Puy-de-Dôme district and by the BRGM Research Division (PREVOIR project). Dr H.M. Kluijver revised the final English version of this MS.

References

Aeschbach-Hertig W., Kipfer R., Hofer M., Imboden D.M., Wieler R., Signer P., 1996, Quantification of gas fluxes from the subcontinental mantle: The example of Laacher See, a maar lake in Germany, *Geochimica et Cosmochimica Acta*, *60*(1), 31-41.

Aeschbach-Hertig W., Hofer M., Kipfer R., Imboden D.M., Wieler R., 1999, Accumulation of mantle gases in a permanently stratified volcanic lake (Lac Pavin, France), *Geochimica et Cosmochimica Acta*, *63*(19/20), 3357-3372.

Batard F., Baubron J.C., Bosch B., Marcé A., Risler J.J., 1982, Isotopic identification of gases of a deep origin in French thermomineral waters, *Journal of Hydrology 56*, 1-21.

Battani A., Deville E., Faure J.L., Noirez S., Tocqué E., Jeandel E., Benoît Y., Schmitz J., Parlouar D., Gal F., Le Pierrès K., Brach M., Braibant G., Bény C., Pokryszka Z., Charmoille A., Bentivegna G., Pironon J., de Donato P., Garnier C., Cailteau C., Barrès O., Radilla G., Bauer A., 2010, Geochemical study of the natural CO2 emissions in the French Massif Central: How to predict origin, processes and evolution of CO_2 leakage, *Oil and Gas Science Technology*, *65*, 615-633.

Beaubien S.E., Ciotoli G., Coombs P., Dictor M. C., Krüger M., Lombardi S., Pearce J.M., West J.M., 2008, The impact of a naturally occurring CO_2 gas vent on the shallow ecosystem and soil chemistry of a Mediterranean pasture (Latera, Italy), *International Journal of Greenhouse Gas Control*, *2*(3), 373-387.

Blavoux B., Dazy J., 1990, Caractérisation d'une province à CO_2 dans le bassin du Sud-Est de la France, *Hydrogéologie 4*, 241-252.

695 Bloomberg S., Werner C., Rissmann C., Mazot A., Horton T., Gravley D., Kennedy B., Oze C.,
696 2014, Soil CO_2 emissions as a proxy for heat and mass flow assessment, Taupo Volcanic
697 Zone, New Zealand, *Geochemistry Geophysics Geosystems*, *15*, 4885–4904,
698 doi:10.1002/2014GC005327.

699 Boudoire G., Liuzzo M., DiMuro A., Ferrazzini V., Michon L., Grassa F., Derrien A., Villeneuve
700 N., Bourdeu A., Brunet C., Giudice G., Gurrieri S., 2017, Investigating the deepest part of a
701 volcano plumbing system: Evidence for an active magma path below the western flank of
702 Piton de la Fournaise (La Réunion Island), *Journal of Volcanology and Geothermal Research*
703 *341*, 193–207.

704 Bräuer K., Geissler W.H., Kämpf H., Niedermannn S., Rman N., 2016, Helium and carbon
705 isotope signatures of gas exhalations in the westernmost part of the Pannonian Basin (SE
706 Austria/NE Slovenia): Evidence for active lithospheric mantle degassing, *Chemical Geology*,
707 *422*, 60-70.

708 Bräuer K., Kämpf H., Niedermann S., Wetzel H.-U., 2017, Regional distribution pattern of
709 carbon and helium isotopes from different volcanic fields in the French Massif Central:
710 Evidence for active mantle degassing and water transport, *Chemical Geology*, *469*, 4-18.

711 Brombach T., Hunziker J.C., Chiodini G., Cardellini C., Marini L., 2001, Soil diffuse degassing
712 and thermal energy fluxes from the southern Lakki plain, Nisyros (Greece), *Geophysical*
713 *Research Letters*, *28*(1), 69-72.

714 Brousse R., Rançon J.P., Le Garrec M.J., Tempier P., Suire J., Veyret-Mekdjian Y., D'Arcy D.,
715 Périchaud J.J., 1990, Explanatory Notes to the 1:50,000-scale geological map of La Tour-
716 d'Auvergne, BRGM Editions, Orléans, France.

717 Burton M.R., Sawyer G.M., Granieri D., 2013, Deep carbon emissions from volcanoes,
718 *Reviews in Mineralogy and Geochemistry*, *75*(1), 323-354.

719 Camarda M., Gurrieri S., Valenza M., 2006, CO_2 flux measurements in volcanic areas using
720 the dynamic concentration method: Influence of soil permeability, *Journal of Geophysical*
721 *Research*, *111*(B05202) doi:10.1029/2005JB003898.

722 Camarda M., Gurrieri S., Valenza M., 2009, Effects of soil gas permeability and recirculation
723 flux on soil CO_2 flux measurements performed using a closed dynamic accumulation
724 chamber, *Chemical Geology 265*, 387–393.

725 Carapezza M.L., Barberi F., Ranaldi M., Ricci T., Tarchini L., Barrancos J., Fischer C., Granieri
726 D., Lucchetti C., Melian G., Perez N., Tuccimei P., Vogel A., Weber K., 2012, Hazardous gas
727 emissions from the flanks of the quiescent Colli Albani volcano (Rome, Italy), *Applied*
728 *Geochemistry 27*, 1767-1782.

729 Chiodini G., Frondini F., Raco B., 1996, Diffuse emission of CO_2 from the Fossa Crater,
730 Vulcano Island (Italy), *Bulletin of Volcanology*, *58*(1), 41–50.

731 Chiodini G., Cioni R., Guidi M., Raco B., Marini L., 1998, Soil CO_2 flux measurements in
732 volcanic and geothermal areas, *Applied Geochemistry*, *13*(5), 543-552.

733 Chiodini G., Baldini A., Barberi F., Carapezza M.L., Cardellini C., Frondini F., Granieri D.,
734 Ranaldi M., 2007, Carbon dioxide degassing at Latera caldera (Italy): Evidence of geothermal
735 reservoir and evaluation of its potential energy, *Journal of Geophysical Research*,
736 *112*(B12204), doi:10.1029/2006JB004896.

737 Chiodini G., Caliro S., Cardellini C., Granieri D., Avino R., Baldini A., Donnini M., Minopoli C.,
738 2010, Long-term variations of the Campi Flegrei, Italy, volcanic system as revealed by the

739 monitoring of hydrothermal activity, *Journal of Geophysical Research*, *115*(B03205),
740 doi:10.1029/2008JB006258.

741 Czernochowski-Lauriol I., Pauwels H., Vigouroux P., Le Nindre Y.-M., 2003, The French
742 carbogaseous province: an illustration of natural processes of CO_2 generation, migration,
743 accumulation and leakage, In: Gale K., Kaya Y., Editors, Greenhouse gas control technologies,
744 vol. 1. Amsterdam: Pergamon, p. 411–416.

745 Etiope G., Martinelli G., 2002, Migration of carrier and trace gases in the geosphere: an
746 overview, *Physics of the Earth and Planetary Interiors 129*, 185–204.

747 Etiope G., Zwahlen C., Anselmetti F.S., Kipfer R., Schubert C.J., 2010, Origin and flux of a gas
748 seep in the Northern Alps (Giswil, Switzerland), *Geofluids*, *10*, 476-485.

749 Etiope G., 2015, Natural Gas Seepage – The Earth's Hydrocarbon Degassing, Springer Eds.,
750 199 p., DOI 10.1007/978-3-319-14601-0.

751 Evans W.C., Sorey M.L., Kennedy B.M., Stonestrom D.A., Rogie J.D., Shuster D.L., 2001, High
752 CO_2 emissions through porous media: transport mechanisms: and implications for flux
753 measurement and fractionation, *Chemical Geology 177*, 15-29.

754 Favara R., Giammanco S., Inguaggiato S., Pecoraino G., 2001, Preliminary estimate of CO_2
755 output from Pantellaria Island volcano (Sicily, Italy): evidence of active mantle degassing,
756 *Applied Geochemistry 16*, 883-894.

757 Fleischer R.L., Mogro-Campero A., 1978, Mapping of integrated radon emanation for
758 detection of long-distance migration of gases within the Earth: Techniques and Principles,
759 *Journal of Geophysical Research*, *83*(B7), 3539-3549

760 France L., Demacon M., Gurenko A.A., Briot D., 2016, Oxygen isotopes reveal crustal
761 contamination and a large, still partially molten magma chamber in Chaîne des Puys (French
762 Massif Central), *Lithos 260*, 328-338.

763 Fridriksson T., Kristjansson B.R., Armannsson H., Margretardottir E., Olafsdottir S., Chiodini
764 G., 2006, CO_2 emissions and heat flow through soil, fumaroles, and steam heated mud pools
765 at the Reykjanes geothermal area, SW Iceland, *Applied Geochemistry*, *21*, 1551-1569.

766 Frondini F., Chiodini G., Caliro S., Cardellini C., Granieri D., Ventura G., 2004, Diffuse CO_2
767 degassing at Vesuvio, Italy, *Bulletin of Volcanology*, *66*, 642–651.

768 Gal F., Brach M., Braibant G., Jouin F., Michel K., 2011, CO_2 escapes in the Laacher See
769 region, East Eifel, Germany: application of natural analogue onshore and offshore
770 geochemical monitoring, *International Journal of Greenhouse Gas Control 5*, 1099-1118.

771 Gal F., Gadalia A., 2011, Soil gas measurements around the most recent volcanic system of
772 metropolitan France (Lake Pavin, Massif Central), *Comptes Rendus Geosciences 343*, 43-54.

773 Gal F., Brach M., Braibant G., Bény C., Michel K., 2012, What can be learned from natural
774 analogues studies in view of CO2 leakage issues in Carbon Capture and Storage applications?
775 Geochemical case study of Sainte-Marguerite area (French Massif Central), *International*
776 *Journal of Greenhouse Gas Control 10*, 470-485.

777 Gal F., Proust E., Bentivegna G., Leconte S., De Lary de Latour L., Loschetter A., Pokryszka Z.,
778 Collignan B., 2017, What may be the consequences of a CO_2 leakage? Insights from soil gas
779 measurements in an urban area – Clermont-Ferrand, French Massif Central, *Energy Procedia*
780 *114*, 3006-3019.

781 Halmer M.M., Schmincke H.U., Graf H.F., 2002, The annual volcanic gas input into the
782 atmosphere, in particular into the stratosphere: a global data set for the past 100 years,
783 *Journal of Volcanology and Geothermal Research 115*, 511-528.

784 Hermansson P.H., Akerblom G., Chyssler J., Linden A., 1991, Geogas—a carrier or a tracer?
785 Statens Karnbransle Namnd (SKN) Report 51, National Board for Spent Nuclear Fuel,
786 Stockholm, p. 66.

787 Hernández P.A., Pérez N.M., Salazar J.M., Nakai S.I., Notsu K., Wakita H., 1998, Diffuse
788 emission of carbon dioxide, methane, and helium-3 from Teide Volcano, Tenerife, Canary
789 Islands, *Geophysical Research Letters*, *25*(17), 3311-3314.

790 Hernández-Perez P., Notsu K., Tsurumi M., Mori T., Ohno M., Shimoike Y., Salazar J., Pérez
791 N., 2003, Carbon dioxide emissions from soils at Hakkoda, north Japan, *Journal of*
792 *Geophysical Research*, *108*(B4), 2210, doi:10.1029/2002JB001847.

793 Hinkle M., 1994, Environmental conditions affecting concentrations of He, CO_2, O_2 and N_2 in
794 soft gases, *Applied Geochemistry*, *9*, 53-63.

795 Holloway S., Pearce J.M., Hards V.L., Ohsumi T., Gale J., 2007, Natural emissions of CO_2 from
796 the geosphere and their bearing on the geological storage of carbon dioxide, *Energy 32*,
797 1194-1201.

798 Inguaggiato S., Jácome Paz M.P., Mazot A., Delgado Granados H., Inguaggiato C., Vita F.,
799 2013, CO_2 output discharged from Stromboli Island (Italy), *Chemical Geology 339*, 52–60.

800 Jähne B., Heinz G., Dietrich W., 1987, Measurement of the diffusion coefficients of sparingly
801 soluble gases in water, *Journal of Geophysical Research*, *92*(C10), 10767-10776

802 Jézéquel D., Michard G., Viollier E., Agrinier P., Albéric P., Lopes F., Abril G., Bergonzini L.,
803 2015, Carbon Cycle in a Meromictic Crater Lake: Lake Pavin, France, *In* Lake Pavin - History,
804 Geology, Biogeochemistry, and Sedimentology of a Deep Meromictic Maar Lake, Sime-
805 Ngando T., Boivin P., Chapron E., Jézéquel D., Meybeck M. Eds, Springer, 10.1007/978-3-319-
806 39961-4.

807 Judd A., 2005, Gas Emissions from Mud Volcanoes. In: Martinelli G., Panahi B. (eds) Mud
808 Volcanoes, Geodynamics and Seismicity. NATO Science Series (Series IV: Earth and
809 Environmental Series), vol. 51. Springer, Dordrecht.

810 Kerrick D.M., 2001, Present and past non-anthropogenic CO_2 degassing from the solid earth,
811 *Reviews of Geophysics*, *39*(4), 565-585.

812 Krüger M., Jones D., Frerichs J., Oppermann B.I., West J., Coombs P., Green K., Barlow T.,
813 Lister R., Shaw R., Strutt M., Möller I., 2011, Effects of elevated CO_2 concentrations on the
814 vegetation and microbial populations at a terrestrial CO_2 vent at Laacher See, Germany,
815 *International Journal of Greenhouse Gas Control*, *5*, 1093-1098.

816 Kämpf H., Bräuer K., Schumann J., Hahne K., Strauch G., 2013, CO_2 discharge in an active,
817 non-volcanic continental rift area (Czech Republic): Characterisation ($\delta^{13}C$, $^3He/^4He$) and
818 quantification of diffuse and vent CO_2 emissions, *Chemical Geology*, *339*, 71-83.

819 Lewicki J.L., Bergfeld D., Cardellini C., Chiodini G., Granieri D., Varley N., Werner C., 2005,
820 Comparative soil CO_2 flux measurements and geostatistical estimation methods on Masaya
821 volcano, Nicaragua, *Bulletin of Volcanology*, *68*, 76-90.

822 Lewicki J.L., Birkholzer J., Tsang C.-F., 2007, Natural and industrial analogues for leakage of
823 CO_2 from storage reservoirs: identification of features, events, and processes and lessons
824 learned, *Environmental Geology*, *52*, 457-467.

825 Liuzzo M., Di Muro A., Giudice G., Michon L., Ferrazzini V., Gurrieri S., 2015, New evidence of
826 CO_2 soil degassing anomalies on Piton de la Fournaise volcano and the link with volcano
827 tectonic structures, *Geochemistry Geophysics Geosystems*, *16*, 4388–4404,
828 doi:10.1002/2015GC006032.

829 Meybeck M., 2015, Pavin, the Birthplace of French Limnology (1770–2012), and Its Degassing
830 Controversy (1986–2016), *In* Lake Pavin - History, Geology, Biogeochemistry, and
831 Sedimentology of a Deep Meromictic Maar Lake, Sime-Ngando T., Boivin P., Chapron E.,
832 Jézéquel D., Meybeck M. Eds, Springer, 10.1007/978-3-319-39961-4.

833 Mörner N.-A., Etiope G., 2002, Carbon degassing from the lithosphere, *Global and Planetary*
834 *Change 33*, 185-203.

835 Notsu K., Mori T., Chanchah Do Vale S., Kagi H., Ito T., 2006, Monitoring quiescent volcanoes
836 by diffuse CO_2 degassing: case study of Mt. Fuji, Japan, *Pure Applied Geophysics 163*, 825-
837 835.

838 Oertel C., Matschullat J., Zurba K., Zimmermann F., Erasmi S., 2016, Greenhouse gas
839 emissions from soils — A review, *Chemie der Erde 76*, 327–352.

840 Parkin T.B., Kaspar T.C., 2003, Temperature controls on diurnal carbon dioxide flux:
841 implications for estimating soil carbon loss, *Soil Science Society of America Journal 67*, 1763–
842 1772.

843 Parkin T.B., Venterea R.T., 2010, Sampling Protocols – Chapter 3 – Chamber-Based Trace Gas
844 Flux Measurements, *In* Sampling Protocols. R.F. Follett editor, 3-1 to 3-39.

845 Pearce J., Czernichowski-Lauriol I., Lombardi S., Brune S., Nador A., Baker J., Pauwels H.,
846 Hatziyannis G., Beaubien S., Faber E., 2004, A review of natural CO_2 accumulations in Europe
847 as analogues for geological sequestration, *Geological Society*, *London*, *Special Publications*,
848 *233*, 29-41.

849 Pedone M., Viveiros F., Aiuppa A., Giudice G., Grassa F., Gagliano A.L., Francofonte V.,
850 Ferreira T., 2015, Total (fumarolic + diffuse soil) CO_2 output from Furnas volcano, *Earth*,
851 *Planets and Space 67*:174.

852 Pokryszka Z., Adelise F., Farret R., Lafortune S., Michel E., Rupasinghe S., 2017, Valeurs de
853 référence du flux de CO_2 et de CH_4 d'origine naturelle biogénique des sols, Rapport INERIS
854 DRS-17-164646-05731A, 48 p.,
855 https://www.ineris.fr/sites/ineris.fr/files/contribution/Documents/INERIS_DRS-17-164646-
856 05731_Referentiel-flux-CO2-CH4-sols_ZPo.pdf

857 Rinaldi A.P., Vandemeulebrouck J., Todesco M., Viveiros F., 2012, Effects of atmospheric
858 conditions on surface diffuse degassing, *Journal of Geophysical Research*, *117*(B11201),
859 doi:10.1029/2012JB009490.

860 Roberts J.J., Wood R.A., Haszeldine R.S., 2011, Assessing the health risks of natural CO_2 seeps
861 in Italy, *PNAS*, *108*(40), 16545-16548.

862 Rogie J.D., Kerrick D.M., Chiodini G., Frondini F., 2000, Flux measurements of non-volcanic
863 emission from some vents in central Italy, *Journal of Geophysical Research*, *105*(B4), 8435-
864 8445.

865 Romanak K.D., Bennett P.C., Yang C., Hovorka S.D., 2012, Process-based approach to CO_2
866 leakage detection by vadose zone gas monitoring at geologic CO_2 storage sites, *Geophysical*
867 *Research Letters 39*, L15405.

868 Sinclair A.J., 1974, Selection of thresholds in geochemical data using probability graphs,
869 *Journal of Geochemical Exploration*, *3*, 129-149.

870 Smith A.Y., Barretto P.M.C., Pournis S., 1976, Radon methods in uranium exploration, IAEA
871 paper SM-208/52, in Exploration for uranium ore deposits – Proceedings of a symposium
872 held in Vienna, 29 March – 2 April 1976, organized by IAEA and NEA (OECD), IAEA
873 SI/PUB/434, ISBN 92-0-040076-0.

874 Sorey M.L., Evans W.C., Kennedy B.M., Farrar C.D., Hainsworth L.J., Hausback B., 1998,
875 Carbon dioxide and helium emissions from a reservoir of magmatic gas beneath Mammoth
876 Mountain, California, *Journal of Geophysical Research 103*(B7), 15303-15323.

877 Toutain J.P., Baubron J.C., 1999, Gas geochemistry and seismotectonics: a review,
878 *Tectonophysics 304*, 1–27.

879 Viveiros F., Ferreira T., Vieira J.C., Silva C., Gaspar J.L., 2008, Environmental influences on soil
880 CO_2 degassing at Furnas and Fogo volcanoes (São Miguel Island, Azores archipelago), *Journal*
881 *of Volcanology and Geothermal Research*, *177*(4), 883-893.

882 Viveiros F., Ferreira T., Silva C., Gaspar J.L., 2009, Meteorological factors controlling soil
883 gases and indoor CO_2 concentration: A permanent risk in degassing areas, *Science of the*
884 *Total Environment 407*, 1362-1372.

885 Viveiros F., Cardellini C., Ferreira T., Caliro S., Chiodini G., Silva C., 2010, Soil CO_2 emissions at
886 Furnas volcano, São Miguel Island, Azores archipelago: Volcano monitoring perspectives,

887 geomorphologic studies, and land use planning application, *Journal of Geophysical Research*,
888 *115 (B12208)*, doi:10.1029/2010JB007555.

889 Viveiros F., Vandemeulebrouck J., Rinaldi A.P., Ferreira T., Silva C., Cruz J.V., 2014, Periodic
890 behavior of soil CO_2 emissions in diffuse degassing areas of the Azores archipelago:
891 Application to seismovolcanic monitoring, *Journal of Geophysical Research Solid Earth*, *119*,
892 7578-7597, doi:10.1002/2014JB011118.

893 Weiss R.F., 1971, Solubility of helium and neon in water and seawater, *Journal of Chemical*
894 *and Engineering Data*, *16*, 235-241.

895 Weiss R.F., 1974, Carbon dioxide in water and seawater: the solubility of a non-ideal gas,
896 *Marine Chemistry*, *2*, 203-215.

897 Werner C., Brantley S., Boomer K., 2000, CO_2 emissions related to the Yellowstone volcanic
898 system. 2. Statistical sampling, total degassing and transport mechanism, *Journal of*
899 *Geophysical Research*, *105*(B5), 10831-10846.

900 Werner C., Brantley S., 2003, CO_2 emissions from the Yellowstone volcanic system,
901 *Geochemistry Geophysics Geosystems*, *4*(7), 1061, doi:10.1029/2002GC000473.

902 Werner C., Evans W.C., Poland M., Tucker D.S., Doukas M.P., 2009, Long-term changes in
903 quiescent degassing at Mount Baker Volcano, Washington, USA; Evidence for a stalled
904 intrusion in 1975 and connection to a deep magma source, *Journal of Volcanology and*
905 *Geothermal Research 186*, 379–386.

906 Werner C., Bergfeld D., Farrar C.D., Doukas M.P., Kelly P.J., Kern C., 2014, Decadal-scale
907 variability of diffuse CO_2 emissions and seismicity revealed from long-term monitoring

908 (1995–2013) at Mammoth Mountain, California, USA, *Journal of Volcanology and*
909 *Geothermal Research*, *289*, 51–63.

Figure captions

Figure 1: Location of the study area.

Top: Location of soil-gas sampling sites (red squares) performed around Lake Pavin (Gal and Gadalia, 2011).

Bottom: Detailed view of the Escarot site: yellow arrows indicate the precise position of the mofette as defined in the 2011 paper and the piezometer defined as a "wet mofette" by Bräuer et al. (2017). Sampling sites of soil-gas flux and soil-gas concentration in June 2017 are indicated by blacked and concentric circles, respectively. Blue pictograms show areas where gas bubbles are observed in stagnant surface puddles.

Background satellite view from Google Earth.

Figure 2: Typology of the flux emissions (CO_2 flux and O_2 depletion).

Point A15 show regular CO_2 enrichment inside the chamber; points A8 and Z16 show short-term variations of the CO_2 enrichment; point E12 show quick sensor saturation; point Z32 show decrease of the CO_2 concentration over time; points BZ8 and E12 show O_2 depletion. Location of the measurement points is indicated on the satellite view.

Figure 3: Top: Atmospheric meteorological conditions (air temperature, atmospheric pressure, wind speed and amount of precipitation) just before before and during the June 2017 survey, on an hourly basis (data from Laqueuille weather station http://www.meteociel.fr/climatologie/villes.php?code=204&mois=6&annee=2017).

Bottom: Detailed view of the survey parameters; temperature, pressure and relative humidity data from the sensors mounted on the flux chamber are indicated by black, red and green dots, respectively.

Figure 4: A: Box plots for soil-gas concentrations data – studies from 2008 to 2012. B: Box plots for soil-gas concentrations data – 2017 study. C: Box plots for soil CO_2 flux. 1: Standard Temperature- and Pressure-corrected data. 2: STP data using steepest slopes in case of fluctuating gas emissions corresponding to gas flushes. 3: STP data corrected to take into account the existence of these gas flushes) and box plot for O_2 depletion. 4. The Coefficient of Variation (CV = Standard Deviation divided by mean value) is indicated for each dataset (in blue).

Figure 5: A: O_2 vs. CO_2 binary plot; dilution lines correspond to the intrusion of CO_2 as a pure phase with end-members corresponding to the CO_2-O_2 composition of the atmosphere, and to the CO_2-O_2 composition of biologically produced CO_2 and consumed O_2 (at 5% and 10% CO_2). B: ^{4}He vs. CO_2 binary plot. C: O_2 depletion vs. STP-normalized CO_2 flux binary plot (domain of biological flux from the synthesis of CO_2 fluxes in France; Pokryszka et al., 2017). Flux data including a gas-flush correction are indicated by yellow stars.

Figure 6: A: CO_2 concentration vs. CO_2 flux binary plot. B: ^{4}He vs. CO_2 flux binary plot; blue triangles: data from June 26th; pink triangles: data from June 27th; green domain: data from Pokryszka et al. (2017); other domains: see text for explanation.

Figure 7: Influence of precipitation events on flux acquisition – see text for explanation. The X-axis shows the duration of the measurement (typically 3 minutes) and the Y-axis shows the increase of CO_2 concentration inside the chamber.

954 *Figure 8: Relation between STP-corrected CO_2 flux and CO_2 flux corrected from gas flushes*
955 *(blue squares), and CO_2 flux corrected from gas flushes and from the effect of precipitation*
956 *events (red squares); green domain: data from Pokryszka et al. (2017).*

957 *Figure 9: Probability plots for CO_2 and helium concentrations, and CO_2 flux. CO_2-flux data are*
958 *considered as measured in the field (normalized to STP conditions) and corrected for*
959 *precipitation influence (see text for the correction procedure). The 2008-2012 dataset refers*
960 *to the entire dataset, i.e. Gal and Galalia (2011) plus some unpublished data from 2012.*

961 *Figure 10: A: Various interpolated maps for CO_2 flux: from left to right: using STP normalized*
962 *data; using STP-normalized data and the gas-flush correction; using additional correction to*
963 *account for precipitation effect. Dashed line shows the NNW-SSE direction.*
964 *B: Interpolated map for O_2 depletion – scale similar to that of CO_2 flux. On the right, part of*
965 *the 1:50,000-scale geological map showing the NNW-SSE fault (dashed line).*
966 *C: From left to right: interpolated maps for CO_2, O_2 and ^4He concentrations in soil gas (dashed*
967 *rectangles show the area used for flux interpolations). All maps were constructed with*
968 *variogram results.*

969 **Table caption**

970 *Table 1: evaluation of CO_2 emissions in the atmosphere; see text for details.*

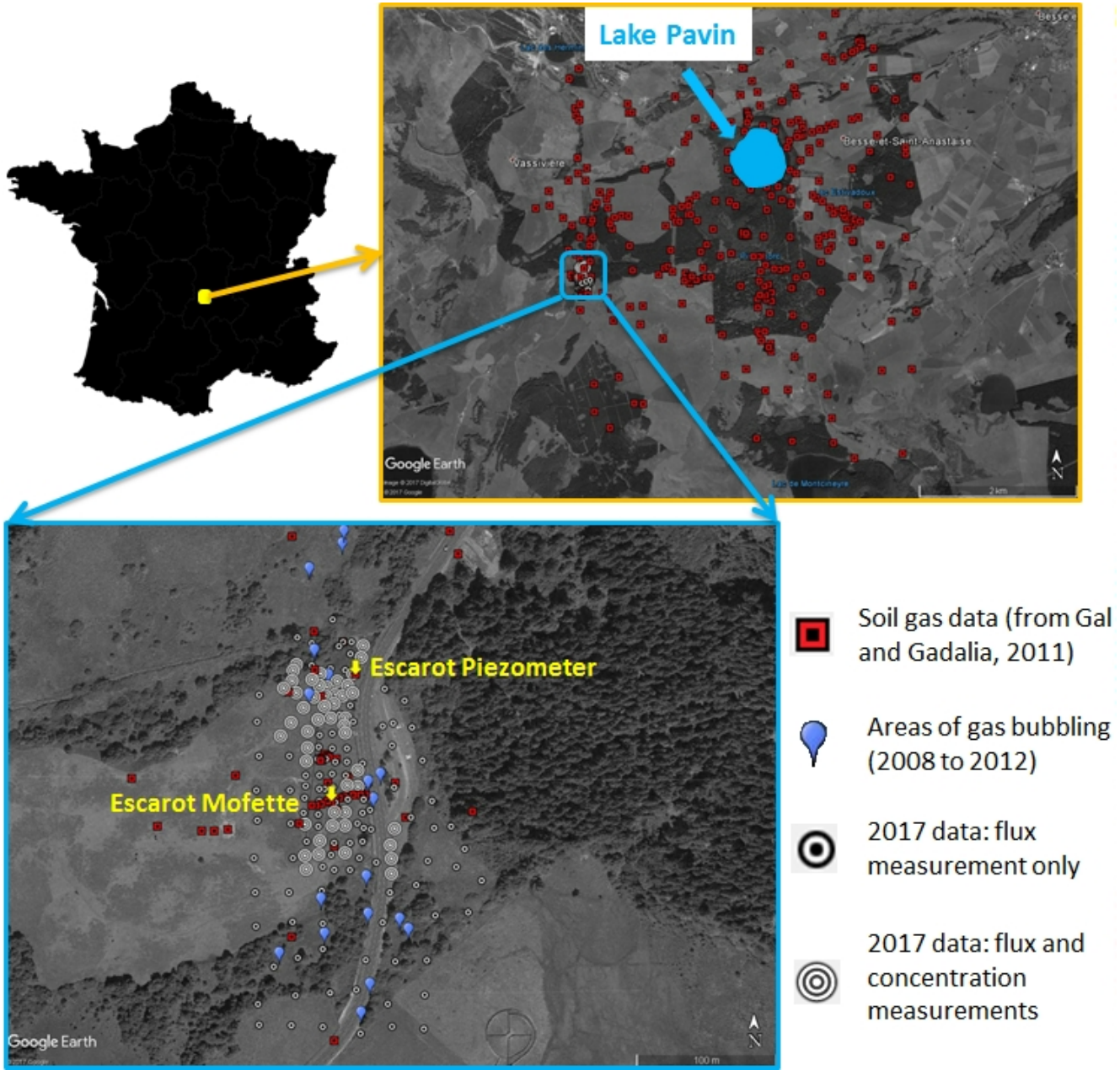
Lake Pavin
Google Earth
Escarot Piezometer
Escarot Mofette
Google Earth
Soil gas data (from Gal and Gadalia, 2011)
Areas of gas bubbling (2008 to 2012)
2017 data: flux measurement only
2017 data: flux and concentration measurements

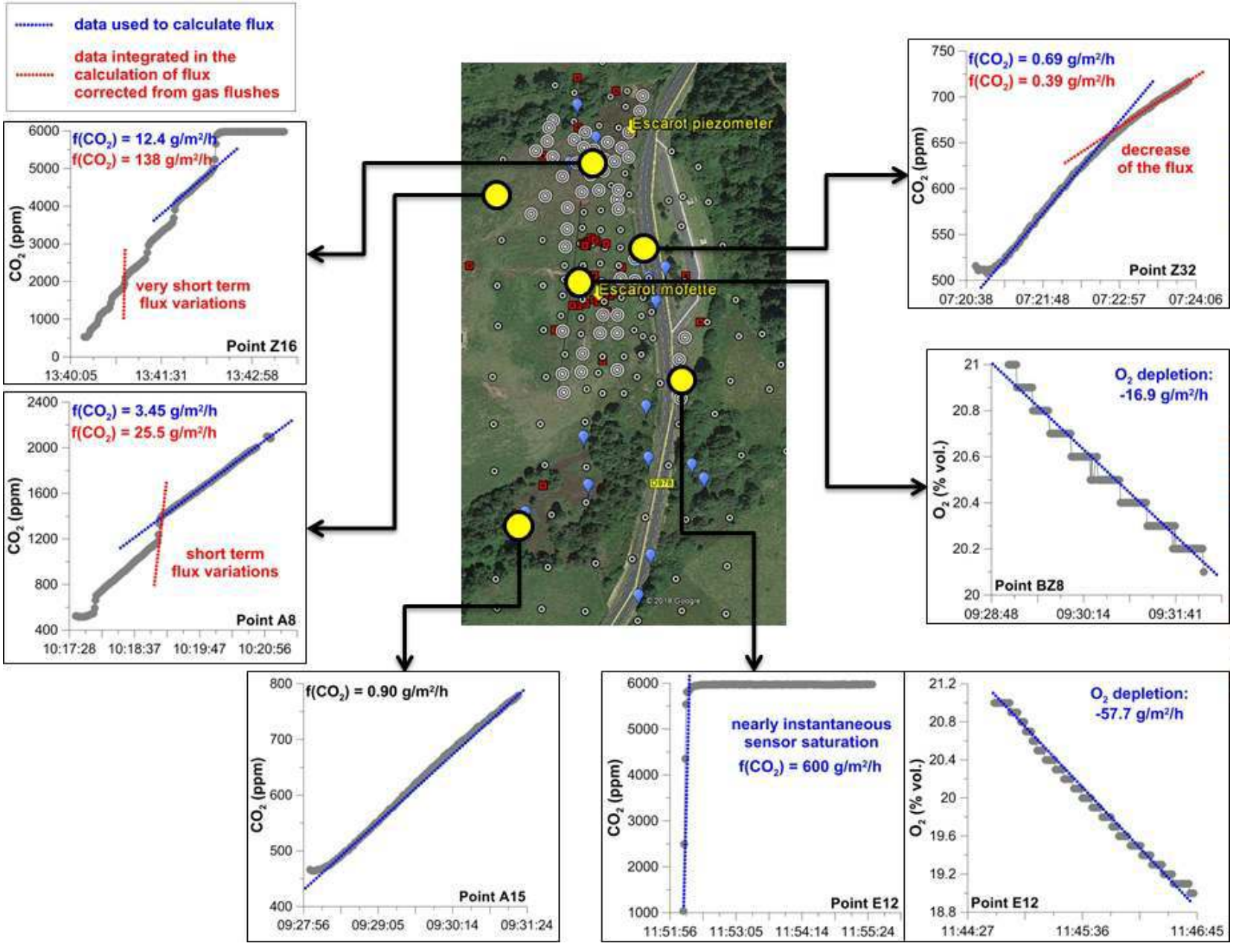
data used to calculate flux
data integrated in the calculation of flux corrected from gas flushes
Escarot piezometer
Escarot mofette
f(CO2) = 12.4 g/m²/h
f(CO2) = 138 g/m²/h
very short term flux variations
Point Z16
CO2 (ppm)
f(CO2) = 0.69 g/m²/h
f(CO2) = 0.39 g/m²/h
decrease of the flux
Point Z32
f(CO2) = 3.45 g/m²/h
f(CO2) = 25.5 g/m²/h
short term flux variations
Point A8
O2 depletion: -16.9 g/m²/h
Point BZ8
O2 (% vol.)
f(CO2) = 0.90 g/m²/h
Point A15
nearly instantaneous sensor saturation
f(CO2) = 600 g/m²/h
Point E12
O2 depletion: -57.7 g/m²/h
Point E12

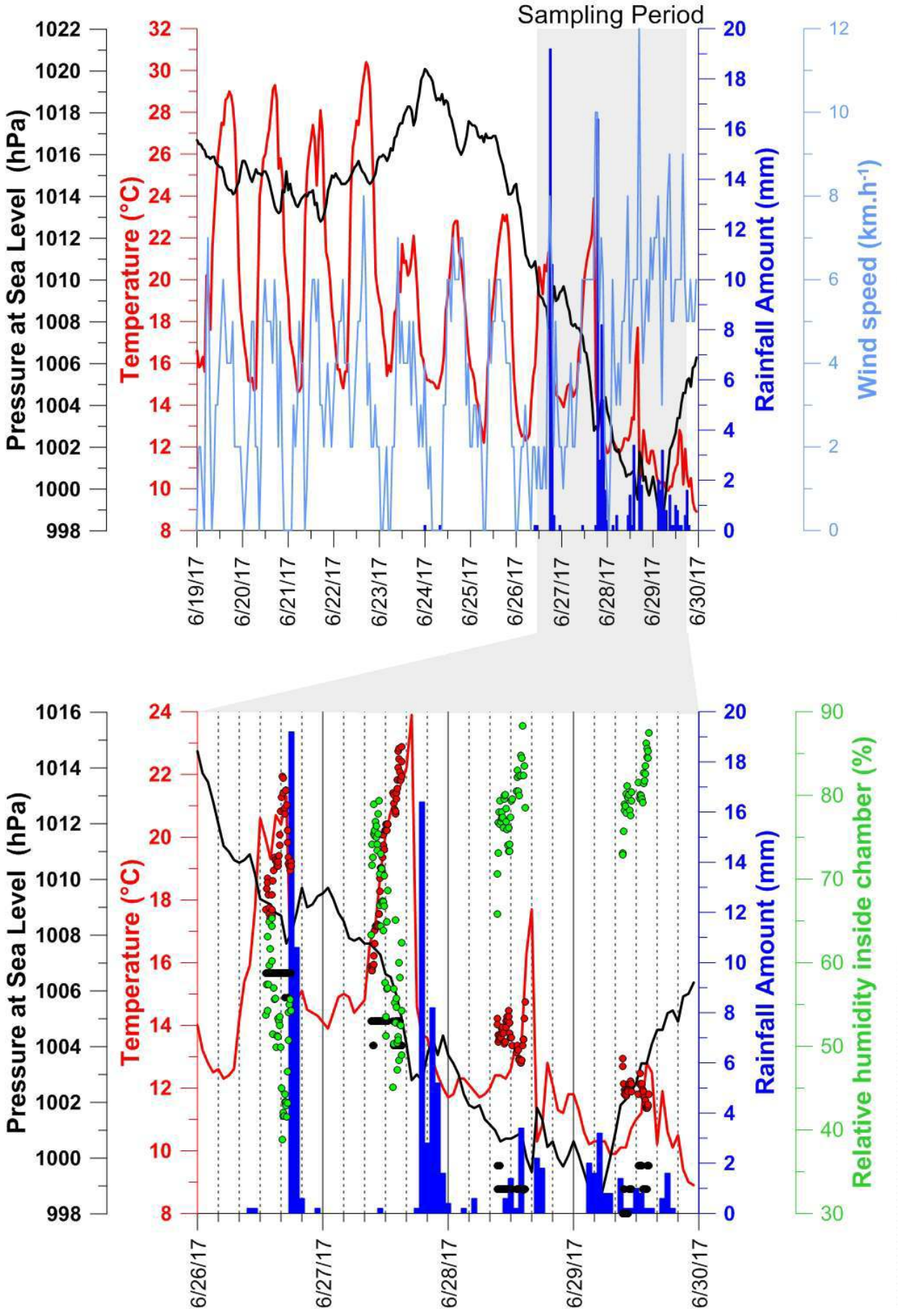
Sampling Period
Pressure at Sea Level (hPa)
Temperature (°C)
Rainfall Amount (mm)
Wind speed (km.h-1)
Relative humidity inside chamber (%)
6/19/17
6/20/17
6/21/17
6/22/17
6/23/17
6/24/17
6/25/17
6/26/17
6/27/17
6/28/17
6/29/17
6/30/17

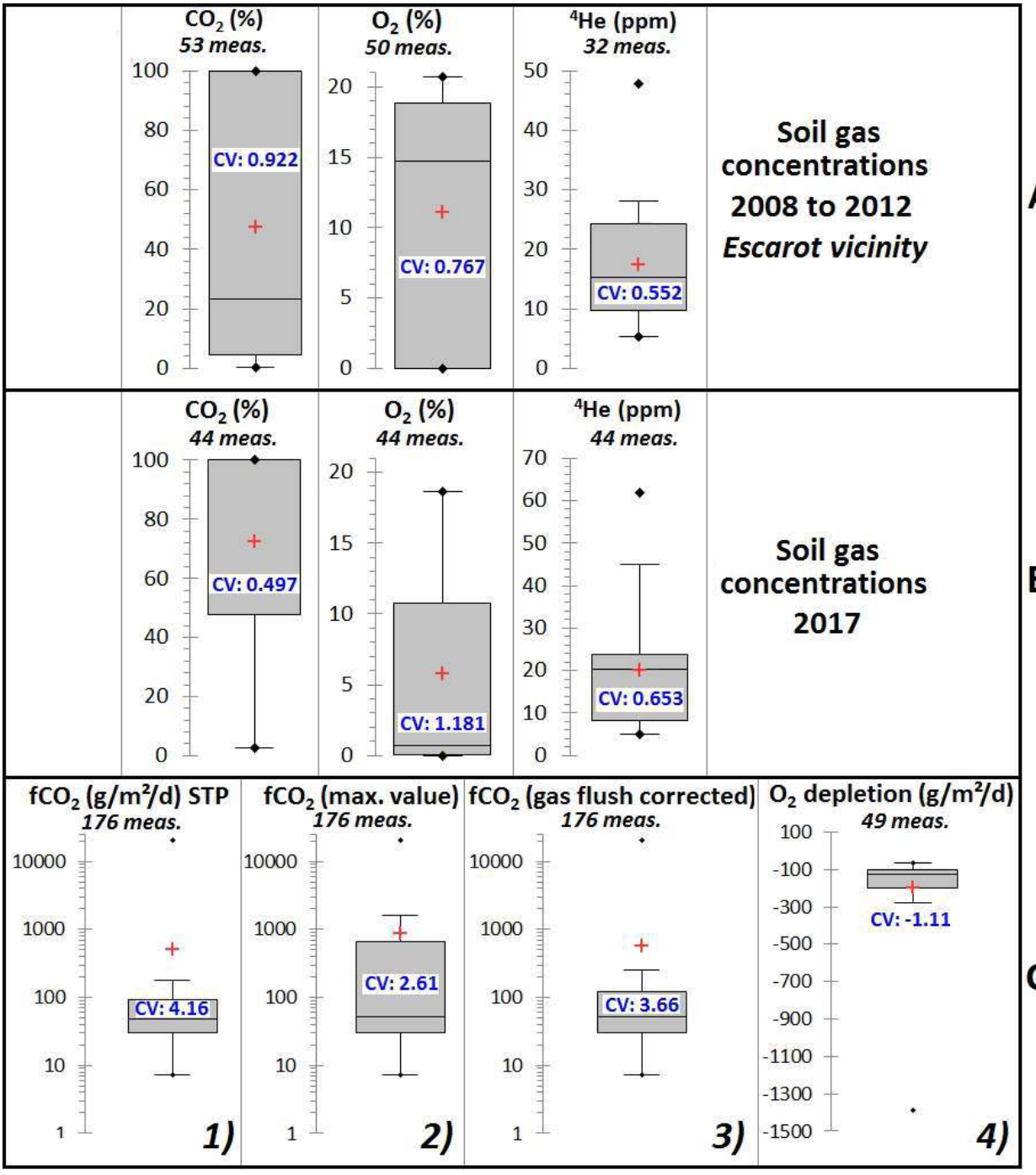
CO2 (%)
53 meas.
CV: 0.922
O2 (%)
50 meas.
CV: 0.767
4He (ppm)
32 meas.
CV: 0.552
Soil gas concentrations 2008 to 2012 Escarot vicinity
A)
CO2 (%)
44 meas.
CV: 0.497
O2 (%)
44 meas.
CV: 1.181
4He (ppm)
44 meas.
CV: 0.653
Soil gas concentrations 2017
B)
fCO2 (g/m²/d) STP
176 meas.
CV: 4.16
1)
fCO2 (max. value)
176 meas.
CV: 2.61
2)
fCO2 (gas flush corrected)
176 meas.
CV: 3.66
3)
O2 depletion (g/m²/d)
49 meas.
CV: -1.11
4)
C)

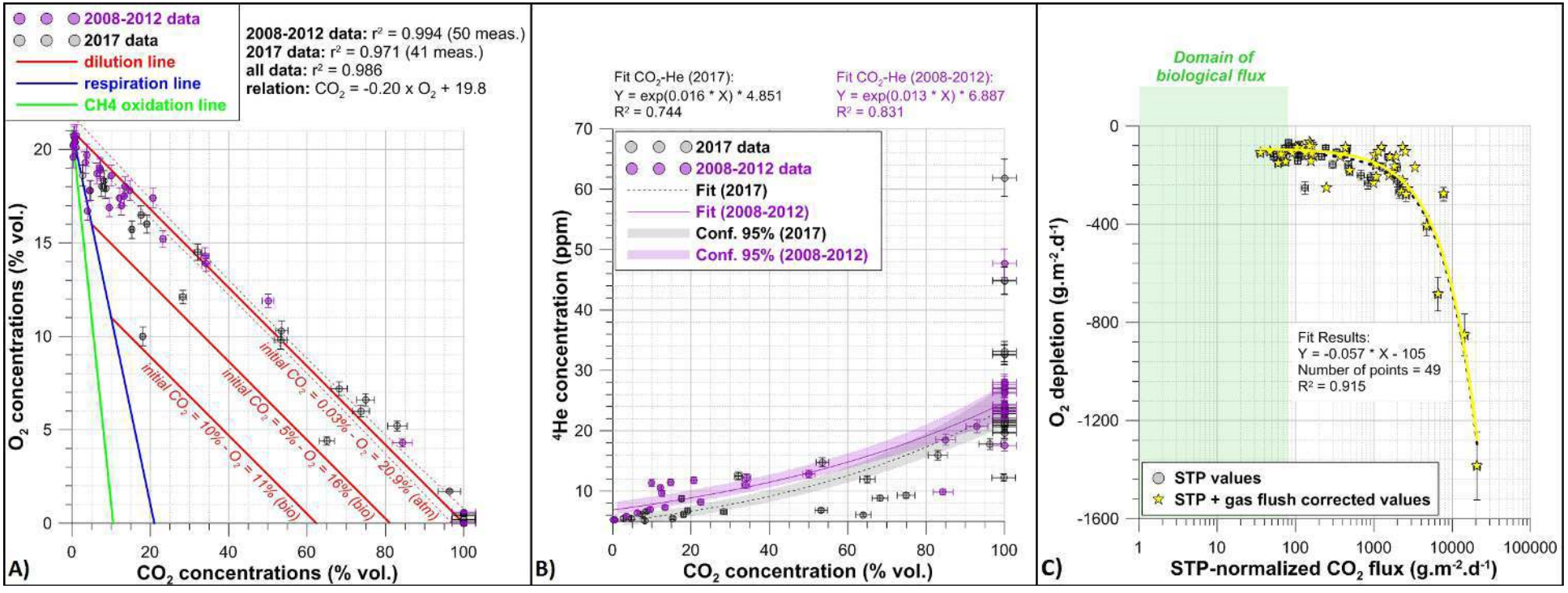
2008-2012 data
2017 data
dilution line
respiration line
CH4 oxidation line
2008-2012 data: r² = 0.994 (50 meas.)
2017 data: r² = 0.971 (41 meas.)
all data: r² = 0.986
relation: CO2 = -0.20 x O2 + 19.8
initial CO2 = 0.03% - O2 = 20.9% (atm)
initial CO2 = 5% - O2 = 16% (bio)
initial CO2 = 10% - O2 = 11% (bio)
O2 concentrations (% vol.)
CO2 concentrations (% vol.)
A)
Fit CO2-He (2017):
Y = exp(0.016 * X) * 4.851
R² = 0.744
Fit CO2-He (2008-2012):
Y = exp(0.013 * X) * 6.887
R² = 0.831
2017 data
2008-2012 data
Fit (2017)
Fit (2008-2012)
Conf. 95% (2017)
Conf. 95% (2008-2012)
4He concentration (ppm)
CO2 concentration (% vol.)
B)
Domain of biological flux
Fit Results:
Y = -0.057 * X - 105
Number of points = 49
R² = 0.915
STP values
STP + gas flush corrected values
O2 depletion (g.m-2.d-1)
STP-normalized CO2 flux (g.m-2.d-1)
C)

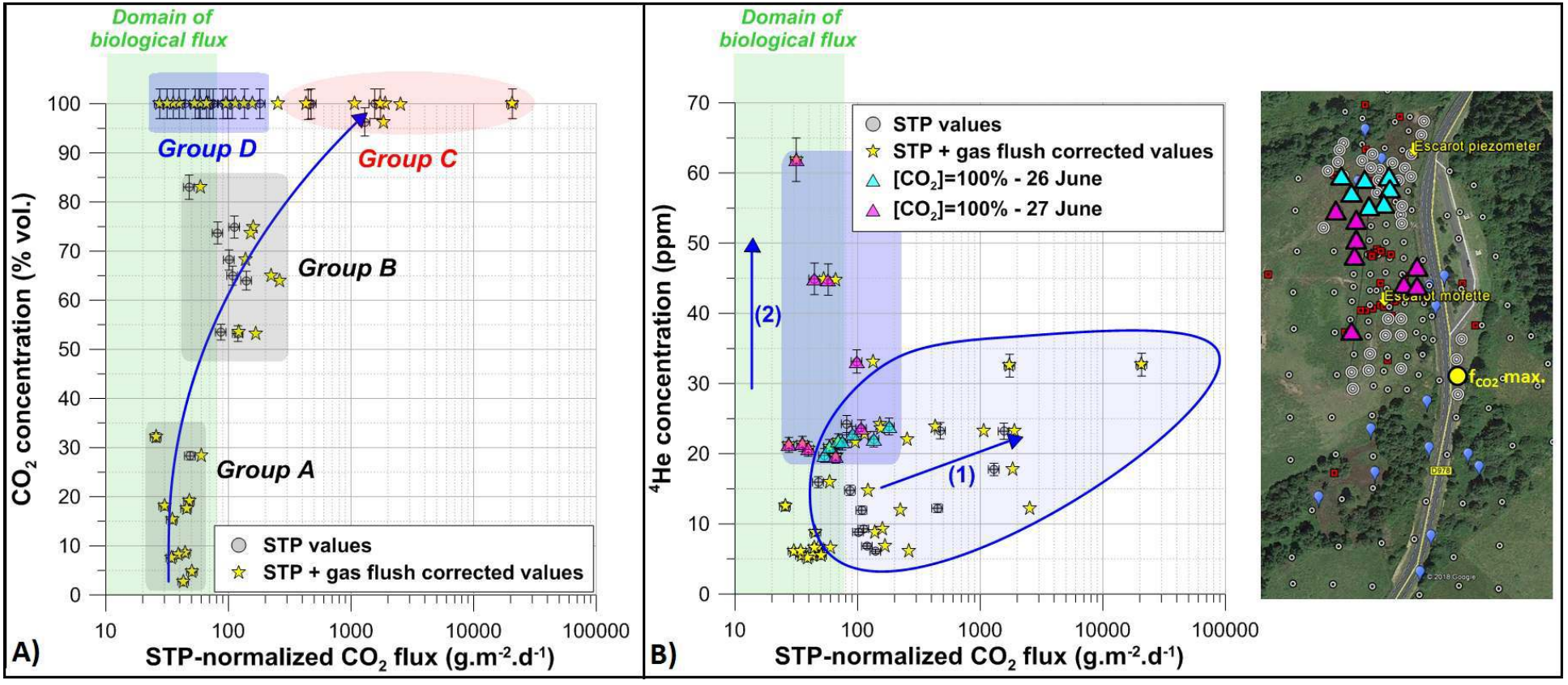
Domain of biological flux
Group D
Group C
Group B
Group A
STP values
STP + gas flush corrected values
CO2 concentration (% vol.)
STP-normalized CO2 flux (g.m-2.d-1)
A)
Domain of biological flux
STP values
STP + gas flush corrected values
[CO2]=100% - 26 June
[CO2]=100% - 27 June
(1)
(2)
4He concentration (ppm)
STP-normalized CO2 flux (g.m-2.d-1)
B)
Escarot piezometer
Escarot mofette
fCO2-max.

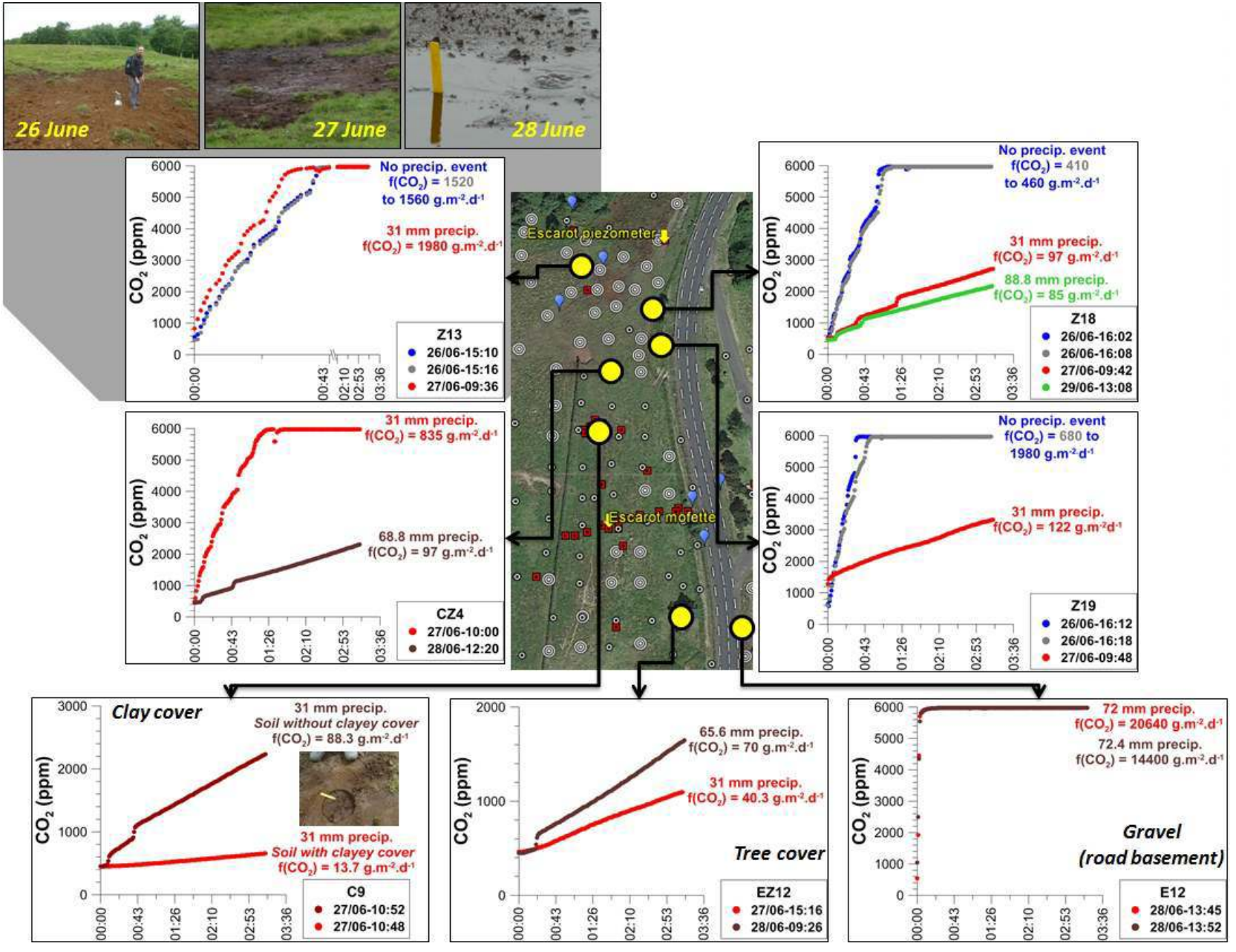
26 June
27 June
28 June
Escarot piezometer
Escarot mofette
No precip. event
f(CO2) = 1520
to 1560 g.m-2.d-1
31 mm precip.
f(CO2) = 1980 g.m-2.d-1
Z13
26/06-15:10
26/06-15:16
27/06-09:36
No precip. event
f(CO2) = 410
to 460 g.m-2.d-1
31 mm precip.
f(CO2) = 97 g.m-2.d-1
88.8 mm precip.
f(CO2) = 85 g.m-2.d-1
Z18
26/06-16:02
26/06-16:08
27/06-09:42
29/06-13:08
31 mm precip.
f(CO2) = 835 g.m-2.d-1
68.8 mm precip.
f(CO2) = 97 g.m-2.d-1
CZ4
27/06-10:00
28/06-12:20
No precip. event
f(CO2) = 680 to
1980 g.m-2.d-1
31 mm precip.
f(CO2) = 122 g.m-2d-1
Z19
26/06-16:12
26/06-16:18
27/06-09:48
Clay cover
31 mm precip.
Soil without clayey cover
f(CO2) = 88.3 g.m-2.d-1
31 mm precip.
Soil with clayey cover
f(CO2) = 13.7 g.m-2.d-1
C9
27/06-10:52
27/06-10:48
65.6 mm precip.
f(CO2) = 70 g.m-2.d-1
31 mm precip.
f(CO2) = 40.3 g.m-2.d-1
Tree cover
EZ12
27/06-15:16
28/06-09:26
72 mm precip.
f(CO2) = 20640 g.m-2.d-1
72.4 mm precip.
f(CO2) = 14400 g.m-2.d-1
Gravel
(road basement)
E12
28/06-13:45
28/06-13:52
CO2 (ppm)
00:00
00:43
01:26
02:10
02:53
03:36

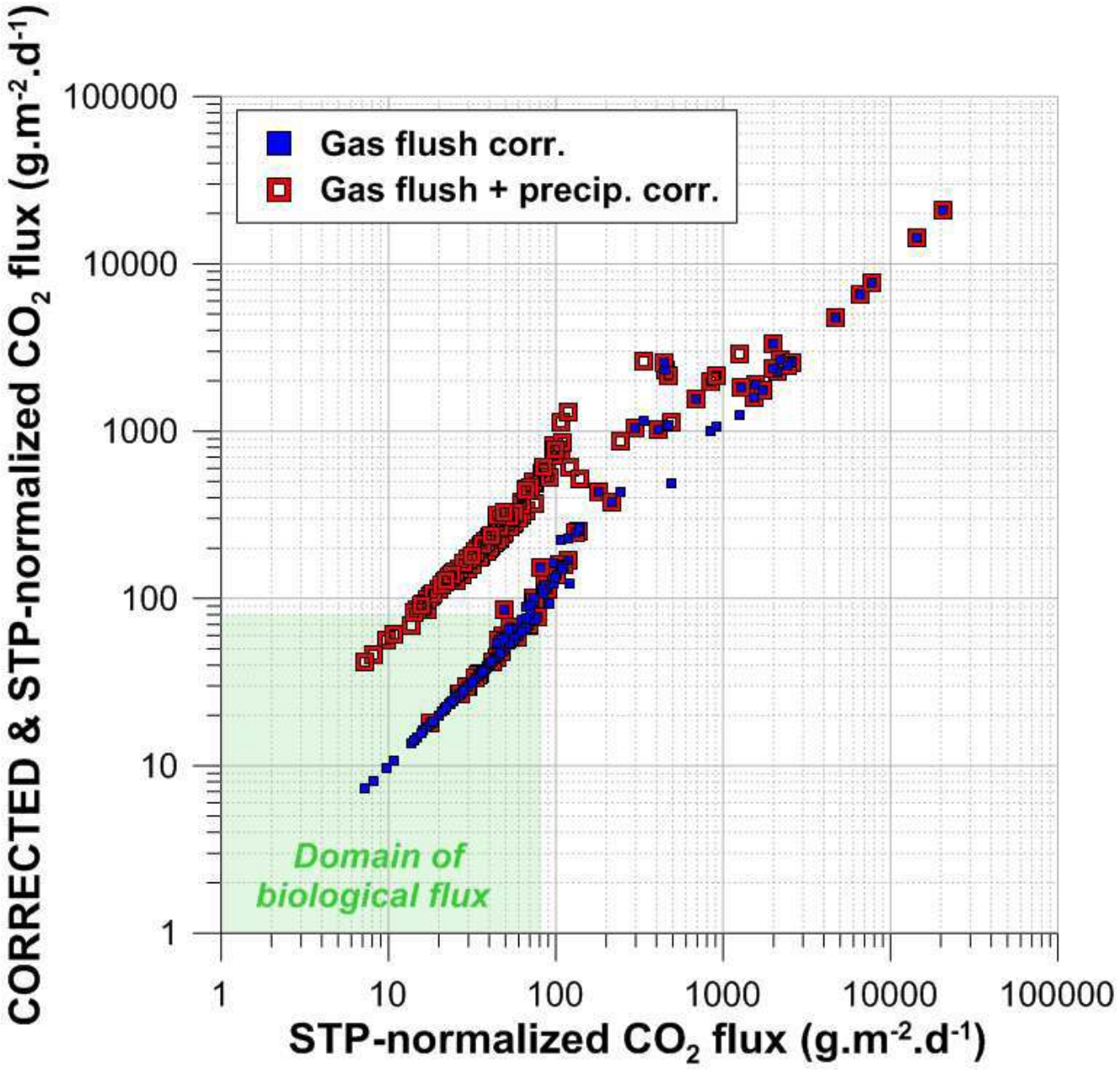
Gas flush corr.
Gas flush + precip. corr.
Domain of biological flux
CORRECTED & STP-normalized CO_2 flux ($g.m^{-2}.d^{-1}$)
STP-normalized CO_2 flux ($g.m^{-2}.d^{-1}$)
100000
10000
1000
100
10
1
1
10
100
1000
10000
100000

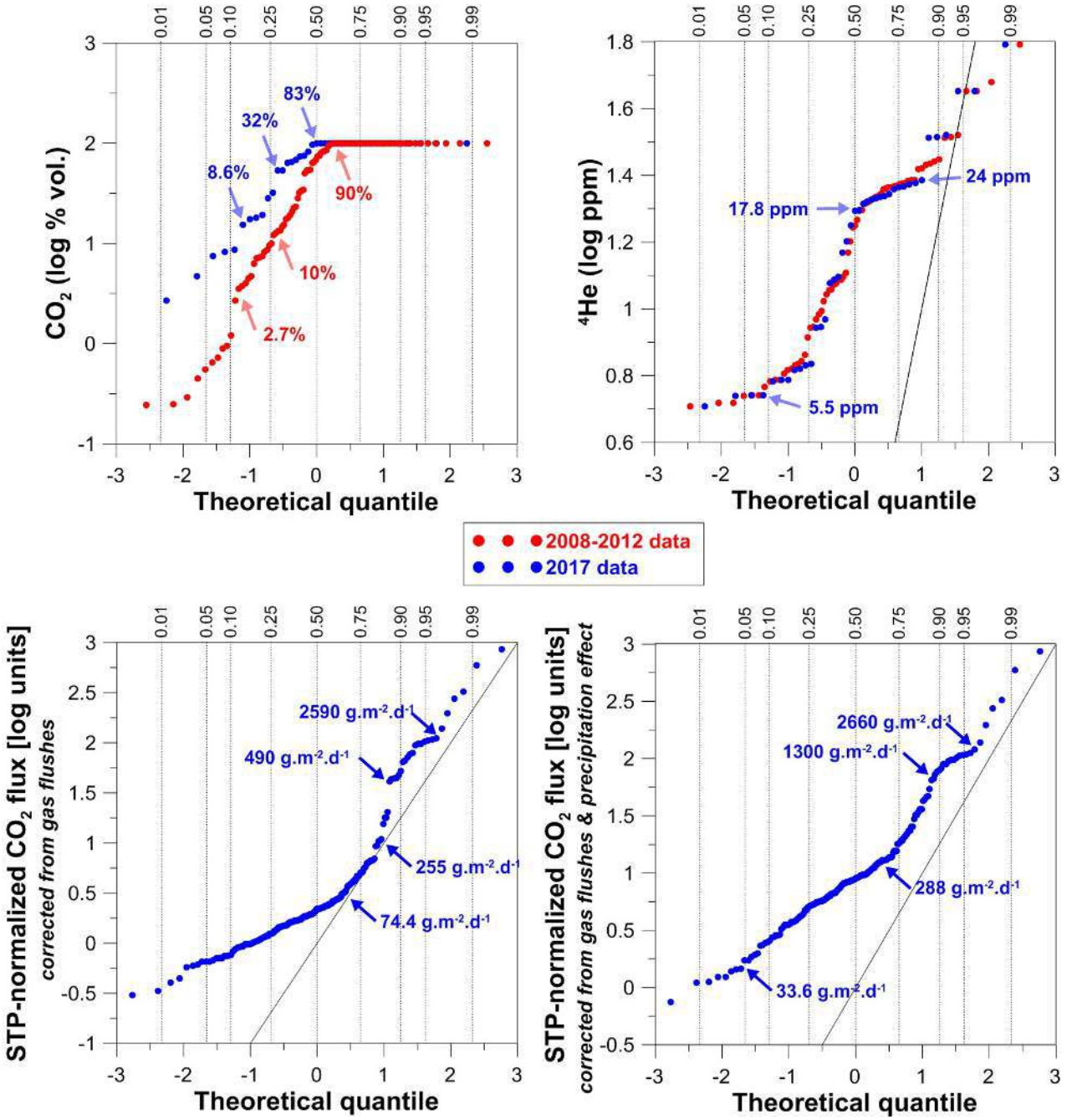
0.01
0.05
0.10
0.25
0.50
0.75
0.90
0.95
0.99
CO2 (log % vol.)
83%
32%
8.6%
90%
10%
2.7%
Theoretical quantile
4He (log ppm)
17.8 ppm
24 ppm
5.5 ppm
Theoretical quantile
2008-2012 data
2017 data
STP-normalized CO2 flux [log units]
corrected from gas flushes
2590 g.m-2.d-1
490 g.m-2.d-1
255 g.m-2.d-1
74.4 g.m-2.d-1
Theoretical quantile
STP-normalized CO2 flux [log units]
corrected from gas flushes & precipitation effect
2660 g.m-2.d-1
1300 g.m-2.d-1
288 g.m-2.d-1
33.6 g.m-2.d-1
Theoretical quantile

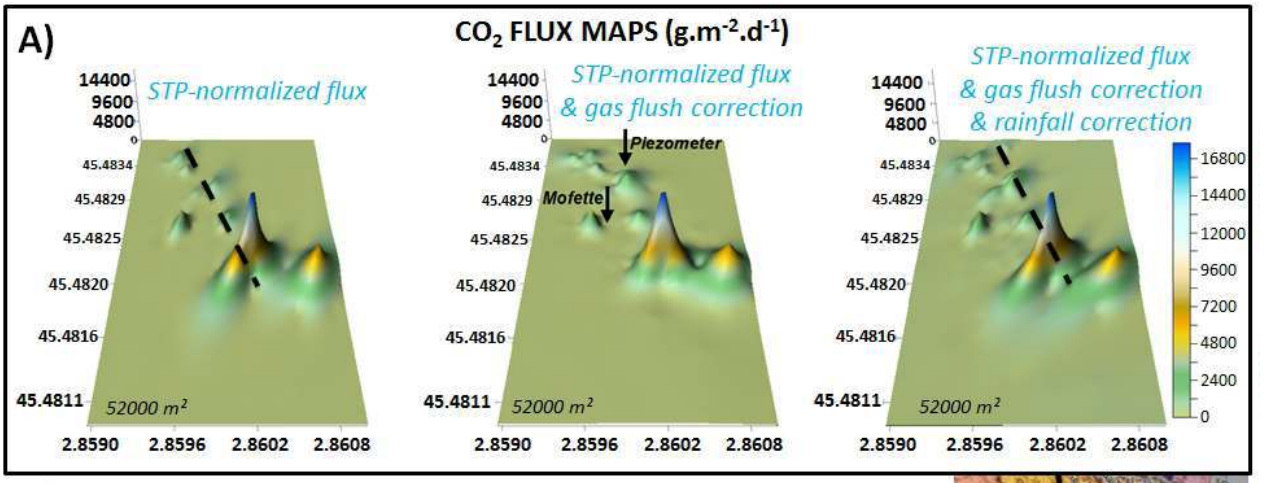
A)
CO_2 FLUX MAPS (g.m^{-2}.d^{-1})
STP-normalized flux
STP-normalized flux & gas flush correction
STP-normalized flux & gas flush correction & rainfall correction
Piezometer
Mofette
52000 m²
14400
9600
4800
0
45.4834
45.4829
45.4825
45.4820
45.4816
45.4811
2.8590
2.8596
2.8602
2.8608
16800
14400
12000
9600
7200
4800
2400
0

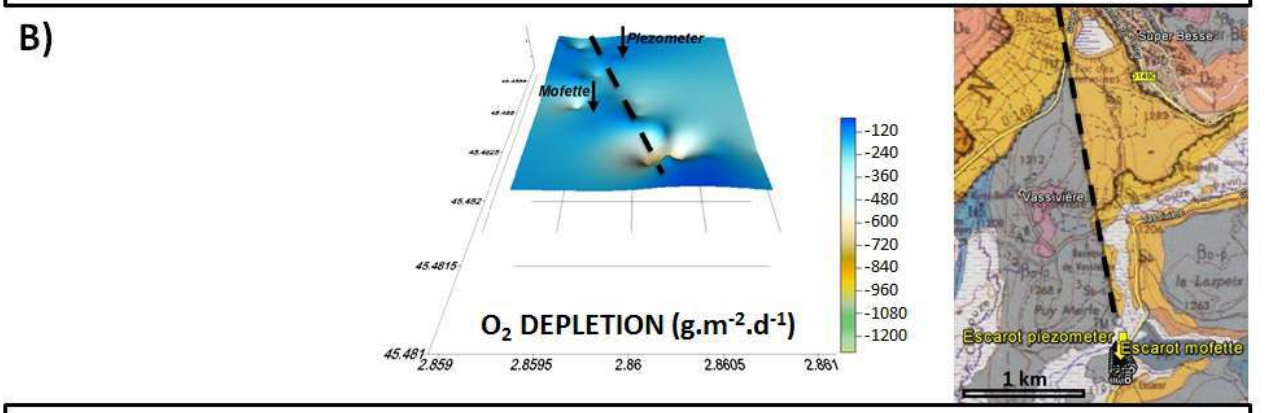
B)
Piezometer
Mofette
O_2 DEPLETION (g.m^{-2}.d^{-1})
-120
-240
-360
-480
-600
-720
-840
-960
-1080
-1200
Escarot piezometer
Escarot mofette
1 km

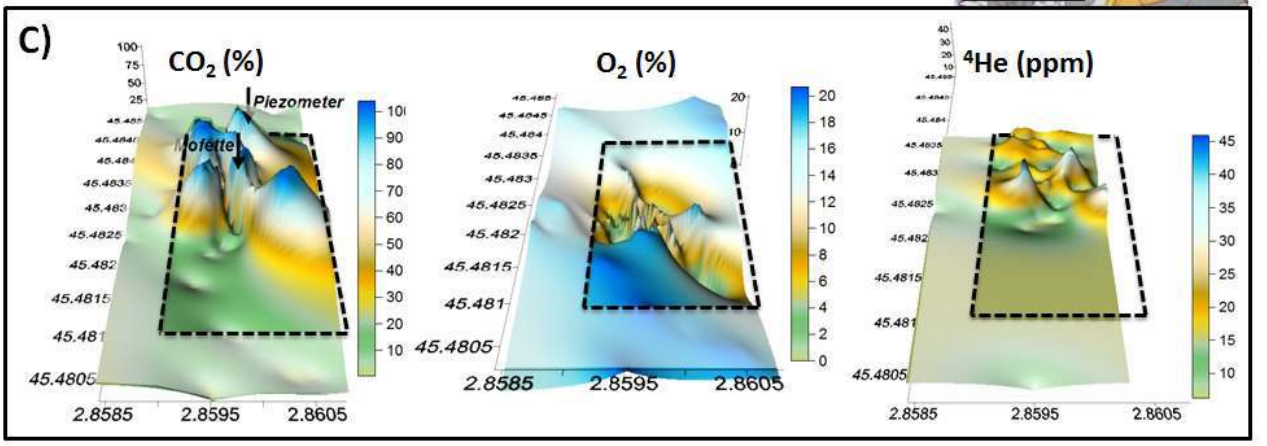
C)
CO_2 (%)
O_2 (%)
^{4}He (ppm)
Piezometer
Mofette
2.8585
2.8595
2.8605

Other emissions to the atmosphere

The rise of deep-seated CO_2 to the surface and its final emission into the atmosphere is not only accompanied by the degassing of other gases, such as helium, but also by the release of chemical elements such as trace metals. This aspect of degassing is less studied than the emission of gases itself, but, *e.g.* Mehlhorn *et al.* (2014) described the consequences of trace-element release/remobilization associated with mofettes, and Bagnato *et al.* (2014) discussed mercury releases associated with volcanic centres. Other work was done for mineral exploration purposes (Pauwels *et al.*, 1999; Castillo *et al.*, 2015; Noble *et al.*, 2017). Here we present some data showing that the Escarot mofette is also prone to such emission of elements. These data were not collected using the approach referring to the use of passive samplers and the adsorption of aerosols; they are the result of a one-day sampling session in February 2009 when a snow cover was present (*Figure A*). We used this snow cover as a natural passive sampler to test if some gases—and thus some chemical elements—can percolate and accumulate in the snow.

On this February day, three locations were investigated. First, the snow cover was removed and the soil-gas atmosphere at 1-m depth was analysed. This allowed defining a location characteristic of the mofette (referred to as Pt200; 100% CO_2 concentration in the soil gas), a location set some metres away, in a less active environment (Pt2000; 22.5% CO_2) and finally a remote location (Pt2001; 0.4% CO_2). Once the soil gas was characterized, we installed PVC pipes at 2 to 3 different levels in the snow cover, to collect snow for subsequent laboratory analyses and to measure the CO_2 concentration once the pipe was removed.

The most interesting results came from Point 200 (*Figure A-A*). The gas phase in the snow cover was influenced by CO_2 release from the mofette: 5 cm above ground level, the

concentration was as high as 10.7%. The concentration then decreaseds to 2.5%, 30 cm above the ground level and to 0.1%, 60 cm above the ground level (or 10 cm below the snow/atmosphere interface). The other two points did not show any enrichment in CO_2 in the snow thus confirming that only areas with high CO_2 fluxes can produce a gas flux that is strong enough to percolate upward into the snow cover.

The concentrations in dissolved elements were also informative (*Figure AB and -C*). Points 2000 and 2001 have similar element concentrations and show little variability with emplacement in the snow cover. Na-Cl contents appear are homogeneous at site scale with a slight tendency of higher contents close to the snow/atmosphere boundary. This may be a consequence of salt spreading on roads, remobilization as dust when the salt has dried and is dispersed by wind. This also highlights that there is no input of Na or Cl from the gas vent. However, enrichment in Ca and K exists for Pt200 5 cm above the soil (enrichment factor: 4 to 5). The concentrations decrease progressively as the distance with soil increases. Similar statements can be made for trace elements such as Pb, Zn, Sr, Cd, Mn, Ni (enrichment factors of 3 at least) and also for Al or As (not shown in *Figure A*1). Some species are not detected at Pt2000 or Pt2001 and are only occur close to the soil surface at Pt200, such as Fe and Cr and Li (not shown in *Figure A*). But these data are too scarce to pretend at a general rule on the release of elements associated to gas seeps, even if they highlight a common behaviour between these two endmembers near the surface.

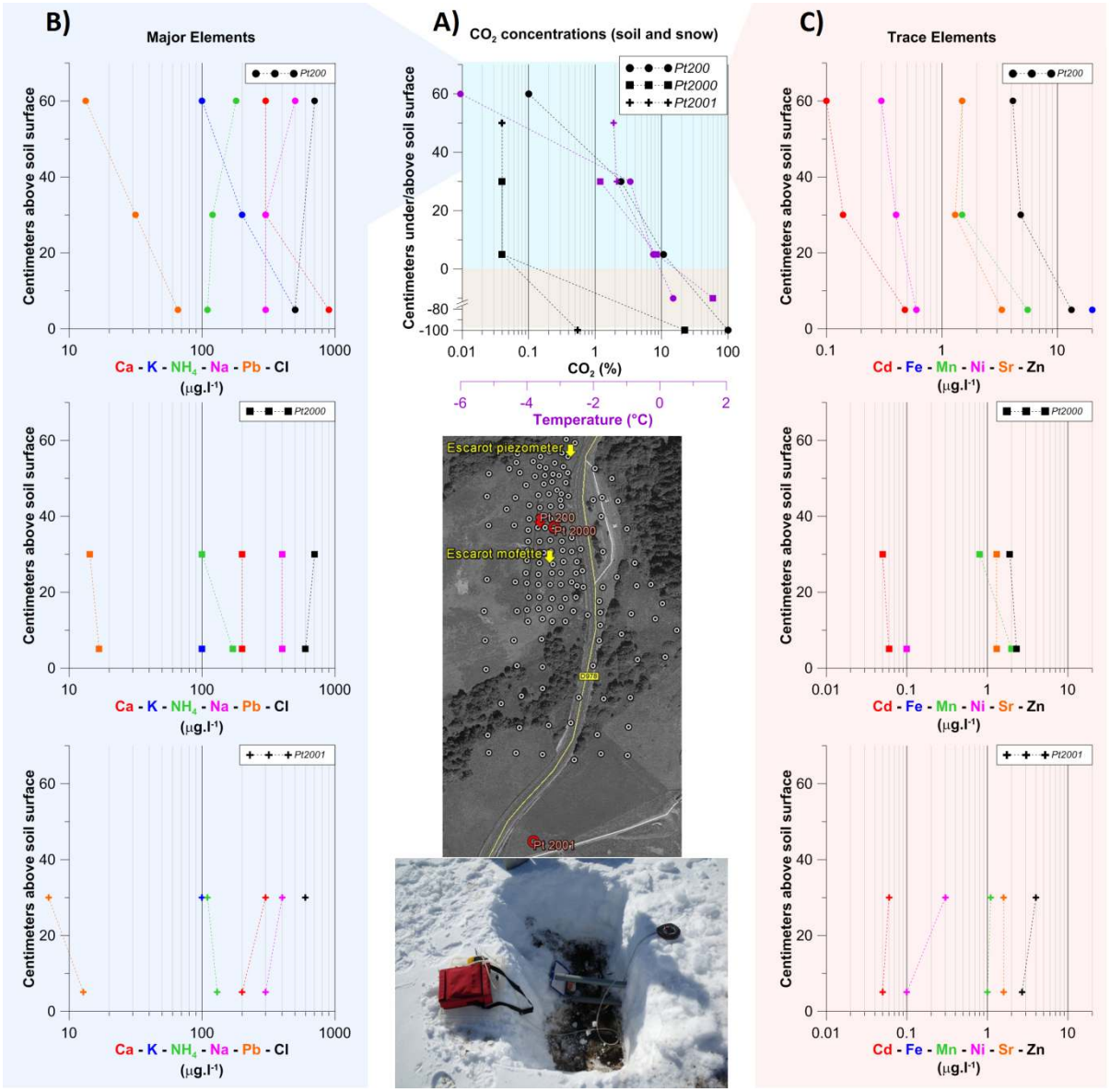

Figure A1: A: CO_2 concentrations in soil (1 m depth) and in the snow cover at 5, 30 and 50 or 60 cm above the ground level as measured on 29 February 2009; temperatures are also indicated – location of the points is plotted on the satellite picture; an overview of the procedure is given in the bottom picture.

B: Some major-element (except Pb) concentrations measured in the snow 5, 30 and 50 or 60 cm above the soil surface.

C: Some trace-element concentrations measured in the snow 5, 30 and 50 or 60 cm above the soil surface.

References:

Bagnato E., Barra M., Cardellini C., Chiodini G., Parello F., Sprovieri M., 2014, First combined flux chamber survey of mercury and CO_2 emissions from soil diffuse degassing at Solfatara of Pozzuoli crater, Campi Flegrei (Italy): Mapping and quantification of gas release, *Journal of Volcanology and Geothermal Research 289*, 26-40.

Castillo P.I.C., Townley B.K., Emery X., Puig A.F., Deckart K., 2015, Soil gas geochemical exploration in covered terrains of northern Chile: data processing techniques and interpretation of contrast anomalies, *Geochemistry: Exploration*, *Environment*, *Analysis*, *15*, 222-233, doi:10.1144/geochem2014-283.

Mehlhorn J., Beulig F., Küsel K., Planer-Friedrich B., 2014, Carbon dioxide triggered metal(loid) mobilisation in a mofette, *Chemical Geology 382*, 54–66.

Noble R.R.P., Seneshen D.M., Lintern M.J., Anand R.R., Pagès A., Pinchand G.T., 2017, Soil-gas and weak partial soil extractions for nickel exploration through transported cover in Western Australia, *Geochemistry: Exploration*, *Environment*, *Analysis*, https://doi.org/10.1144/geochem2017-026.

Pauwels H., Baubron J.-C., Freyssinet P., Chesneau M., 1999, Sorption of metallic compounds on activated carbon: application to exploration for concealed deposits in southern Spain, *Journal of Geochemical Exploration 66*, 115–133.